学位論文(要約)

Study on Two-dimensional π-Conjugated Pd and Pt Dithiolene Polymers

(パラジウムおよび白金の二次元π共役ジチオレン錯体ポリマーの研究)

平成 28 年 7 月博士（理学）申請

東京大学大学院理学系研究科

化学専攻

PAL TIGMANSU

パル ティグマンスー

Abstract

The thesis describes the synthetic strategies of two-dimensional π-conjugated heavier group 10 metal bis(dithiolene) complex nanosheets. I have demonstrated the synthetic problems for such system and the ways to overcome it in order to synthesize such multinuclear 2-D planar framework. In this study, interfacial synthesis of multi-layered films, control over redox potential of ligand, electro-catalytic properties of such films in hydrogen evolution reactions and conductivity were explored.

Chapter 1 deals with the brief introduction of 2-D architectures. I have discussed the importance, classifications and recent developments in the field of 2-D material science.

Chapter 2 deals with the synthetic strategies of the 2-D palladium bis(dithiolene) (**PdDT**) coordination nanosheets. The manipulation of the redox activity of the benzene hexathiol (BHT) ligand has been shown here by use of oxidizing agent. Pristine liquid-liquid interface was exploited for synthesis of thicker stacked coordination sheets; while going for thin layers of sheets, the gas-liquid interface was used. The structure, composition was comprehensively identified by several microscopic and spectroscopic techniques.

Chapter 3 investigates on the synthetic problems on formation of two-dimensional platinum bis(dithiolene) (**PtDT**) nanosheets. The synthetic strategies were modified and novel transmetallation techniques for multi-layer and few layer films were fabricated from the liquid-liquid and the gas-liquid interfaces. The structure, composition, and properties are identified comprehensively using XPS, SEM, AFM, TEM and IR spectroscopy.

Chapter 4 discusses in possibility of further extension of the metalladithiolene framework from group 10 to group 11 metals challenging synthetic difficulties for synthesis of gold nanosheet (**AuDT**). In addition, extensively XPS, TEM and AFM are used for characterization.

Chapter 5 tries to cast some light in brief as a scope for use of such framework in different applications, precisely the conductivity and the electro-catalysis for hydrogen evolution reaction (HER) for group 10 metalladithiolene nanosheet are the prime objectives.

Chapter 6 concludes on present study and remarks on the future prospects of such frameworks.

Contents

Chapter 1

Introduction

1.1 Importance of Dimensionality

In our daily life electronics has been an integral part of our survival. Day by day the devices we depend on are becoming smarter and smaller, rather in other words, the energies are now more precise. Device fabrication with such a precision is simply possible owing to the phenomenon of quantum confinement effects[1] which deals with change in the quantum properties just depending on size of the chemical structure as a result the local behavior of electrons in the discrete energy level changes. Hence, modulation of physical properties of a bulk material can be single handed guided by the factor called dimensionality. The tuning of optics[2 3] and the electronics[4] has been a remarkable fit of achievement as per the continuous energy states limit to discreet bands; thereby resulting into precise use of band gap for device fabrication.

The approach of defining the dimensionality has changed in due course by both theoreticians and experimentalists and has been proved to show unusual physical properties in the fields of electronics[5], spinotronics[6], optonics[7], photonics[8 9], etc. In better understanding as in Figure 1.1 for example, a 0-D can be thought as a single atom or a rather discrete group of caged molecules like fullerenes[10] or non-caged cluster of atoms like QDs[2,4,11] or nanoparticles; similarly, CNTs[12] or 1-D polymers[13 14] can be classified as examples of the 1-D materials. On the other hand, graphene[15,16] being the first 2-D material has intrigued scientists for their unusual properties.

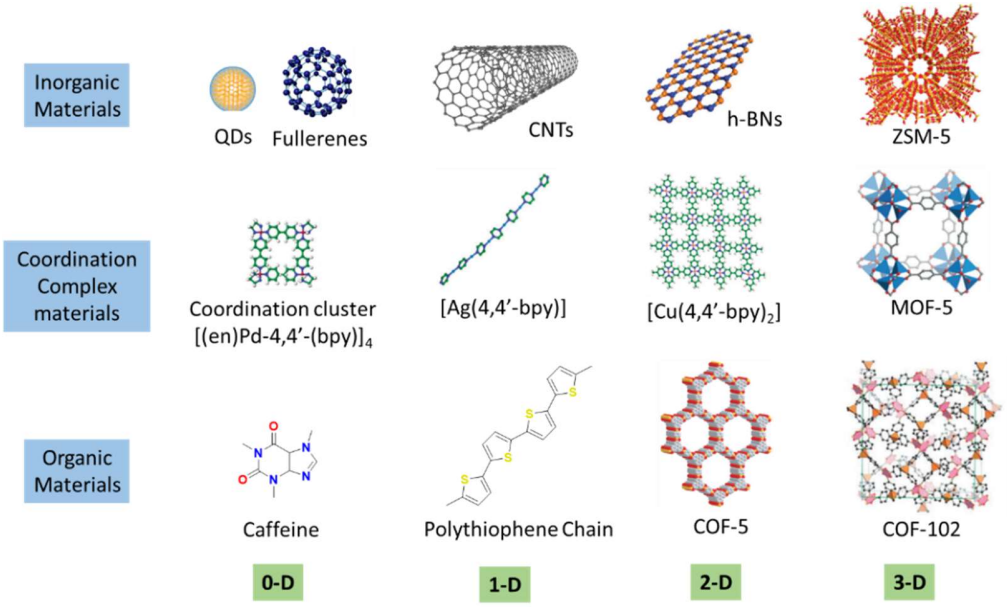

Figure 1.1 Different chemical architectures defining dimensionality.[17]

1.2 Classification of 2-D Layered Materials

Since the confinement of the bulk properties towards lower dimensionality has progressed much of its course, two-dimensional (2D) materials gained significant attention. After the discovery of graphene, interesting physical properties once predicted was seen to be existing, for example, Quantum Hall Effect (QHE)[18,19], which intrigued scientists to research more about the 2-D materials. In fact, in the field of material science and nanoscience, the anisotropy[20] sheer induces the variation in properties; in addition, the thickness (in nm scale) of such material improves the effect further. 2-D layered materials can be classified depending on its composition, synthetic procedure, application to be used for and etc. I would like to classify these layered materials by their composition in order to understand their electronics (dependent on different elements) and their applications (dependent on their energy distributions). Hence, 2-D materials can be categorized as follows: 1) single elemental 2-D layered material (example graphene comprising carbon), 2) inorganic 2-D layered material (example metal oxides, metal dichalcogenides, etc), 3) self-assembled 2-D layered material (metallic nanosheets), and 4) organic 2-D framework.

1.2.1 Single Elemental 2-D Layered Material

The first, of its kind, graphene, which is 2-D network of sp^2 hybridized carbon in hexagonal lattice retaining the extended π-conjugation by aromaticity and discovered in 2004 by Novoselov and Geim[15], was found to be the wonder material. With zero band gap[21,22], it has a very high carrier mobility[5] following the relativistic Dirac equation[23] for electron transport and the observation of half integer Quantum Hall Effect (QHE)[18] made the vintage theories come to life and its charge carriers are massless Dirac fermions[23] proved to be the beginning of new era of 2-D networks. Unfortunately, of not having the bandgap in pristine graphene, sheet makes it harder for electronics as compared to silicon electronics. Although, band gap can be created and tuned by doping[24], π–π stacking of small molecules[25], covalent bonding[26,27] or even increasing the thickness of layers[21] which makes it usable in photonics[8] and optoelectronics[9]. General approach for this kind of single elemental 2-D layered material is by top-down approach, yet nowadays bottom-up approach can be used like wet chemical synthesis[28,29] for graphene and graphdiyne[30]. Graphene's cousins like graphyne[30,31], graphdiyne, graphone[32], and graphane (CH)[33] etc. have been predicted to be the list

of wonder materials, due to their band structure tuning compared to that of graphene, although few of them are yet to be synthesized. Thus, the research for a better 2-D material is essential for electronics.

The other analogues of graphene have been the increasing research in the field of 2-D layered materials. Silicon imprints the sister graphene analogue called as silicene[34–36]. With buckled honeycomb lattice and Dirac band structure[37,38], it is possible to influence the band gap, band structure and nano-electronics by external fields and interface interaction[39]. It has been predicted that the Quantum Spin Hall effect[40–43], chiral superconductivity[44], giant magnetoresistance[45] can be seen in monolayer silicene. Similar to the silicene, germanium analogue named as germanene[46] has also been reported. Multilayer hydrogen terminated germanane[47] (GeH), analogues to graphane structure, can be synthesized both by topochemical deintercalation of $CaGe_2$ and mechanical exfoliation[47].

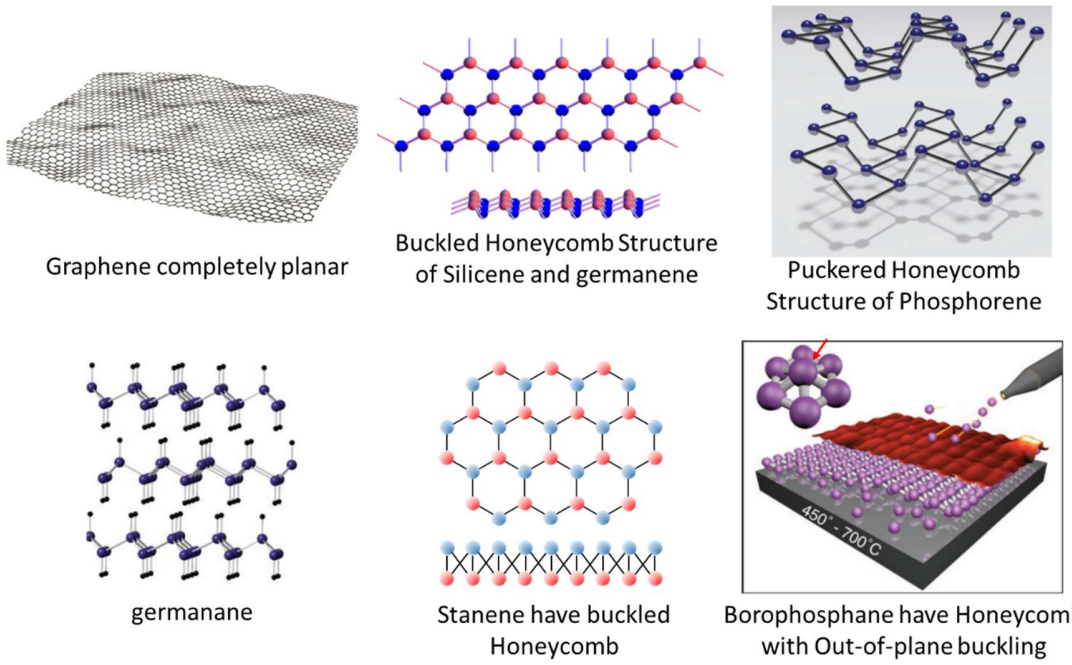

Figure 1.2.1 Structural differences among single elemental 2-D layered material[15,46-48,53,54].

Taking steps with silicon and germanium, phosphorus has emerged with its class of 2-D layered materials called as phosphorene or phosphane[48,49]. The puckered honeycomb structure of phosphorus bonded with other three adjacent phosphorus atom makes a 2-D network. The

monolayer acts as semiconductor and a direct band gap of ~2eV was observed with layered dependent high charge carrier mobility[48] ranging to ~1000 cm^2 $V^{-1}s^{-1}$ for 10nm thick layers. Transistor performance was seen in 7.5-nm thick layers with high order of drain current modulation in the order of 10^5 [50]. As for the other applications optoelectronics[51], anode material for sodium ion batteries[52] and layered dependent photo assisted oxidation[20] and quantum confinement effects[20] were also established for this class of 2-D material. Besides phosphorene, crystalline 2-D boron sheets named as borophene[53] were very recently synthesized where it forms honeycombs of boron atoms with each hexagon capped with another boron atom forming an outer-plane buckling unlike boron nitride (BN)s as in Figure 1.2.1. Along with it was also seen that unlike other allotropes, borophene is found to be metallic[53].

Moving forward from nonmetals like carbon, boron, phosphorus and metalloid like silicon and germanium, metals forming such network might be interesting as band structure is concerned. Recently, tin forming such networks called as stanene[54] has been made successfully by epitaxial growth. The prediction of room temperature QHE with enhanced thermoelectricity[55] and topological superconductivity[56] increases the scope of research for the search of such kind 2-D layered materials. It is interesting to note that group 14 elements are the point of all interest because of their interesting valence shell configurations.

1.2.2 Inorganic 2-D Layered Materials

The top-down approach is substantially important for graphene, its analogue materials and for other kinds of robust inorganic layered materials as the search of the quantum properties is concerned. Boron nitrides[57,58], transition metal dichalcogenides (TMDCs), transition metal oxides and hydroxides, perovskite oxide[141] and transition metal nitriles, carbides or carbonitrides (MXenes) are the class of 2-D materials as in Figure 1.2.2 which are found to be having better properties than graphene due to the presence of direct bandgap for device fabrications.

Monolayers of transition metal dichalcogenides, with direct gap located at K-point, are thin semiconducting layered materials of type MX_2 (M= Bi, Mo, W; X=S, Se, Te)[59–64] can be synthesized from exfoliation of bulk crystal (having indirect bandgap), chemical vapour deposition (CVD)[60] and molecular beam epitaxy[65]. These are important as for transistors[66] and

optoelectronics[67] are concerned. The TMDCs having no inversion center, allowing new degrees of freedom of charge carriers such as k-valley index[61]; hence, as far valleytronics[68] is concerned, this creates an interesting field of research in Physics. Further, strong spin-orbit splitting in monolayer leads to the building of spintronics devices.

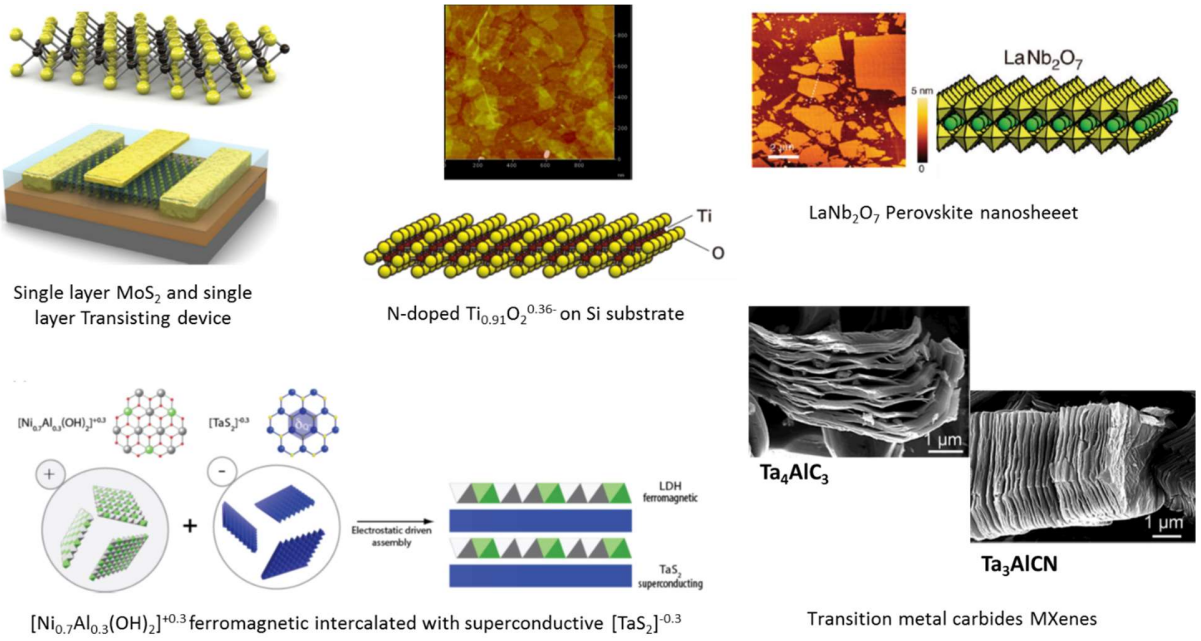

Figure 1.2.2 Different examples of inorganic 2-D layered materials[66,70,76,141,142].

On the other hand, transition metal oxides have been of much importance due to the catalysis[69], photocatalysis[70], electronics, photovoltaics[70], dielectrics and bio medical applications[70], although much of the metal oxides used are based on the titanium and manganese as the metal counter parts. Layered double hydroxides (LDH) of type $[M^{2+}_{1-x}\ Al^{3+}_x(OH)_2]^{x+}$ (M: Mg, Co, Ni, Zn)[71,72] ($0.2 \leq x \leq 0.33$) have redox active magnetic properties[70,142], while choice of metal (M) type would induce properties like photoluminescence in case of type $[RE^{3+}(OH)_{2.5}\ xH_2O]^{0.5+}$ (RE: Nd, Sm, Eu, Gd, Tb, Dy, Ho, Er)[73–75]. Hydrophilic transition metal carbides (MXenes), like titanium carbides[76–78], are promising for high volumetric capacitance[77] and battery applications[78].

1.2.3 Self Assembled 2-D layered material

This class of materials can be considered similar to previous category as in section 1.2.1, containing one single entity or group of entities, yet differs in the fact that the repeating unit forms self-assembled nano-architectures by mere cluster of metals or group of molecules through H-bonding[79,80], van der Waals interaction or ionic interaction. Self-assembly[81,82] of molecules like pyrene[83] or terrylene-based dye[80], forming a bi-component supramolecular network with melamine shows photo response[80] intriguing possibilities in bottom-up fabrication of optoelectronic devices. It is interesting to build supramolecular surface confined pores of different sizes[84], conductive assemblies guided by DNA-strands by H-bonding interactions[85,86] and the host-guest chemistry and its molecular dynamics with the guest molecule, in particular porphyrins[81,87] and its derivatives' interacting with the substrate[79] or guest molecule like heptamers of C_{60}[88] trapped within the cavities as in Figure 1.2.3.

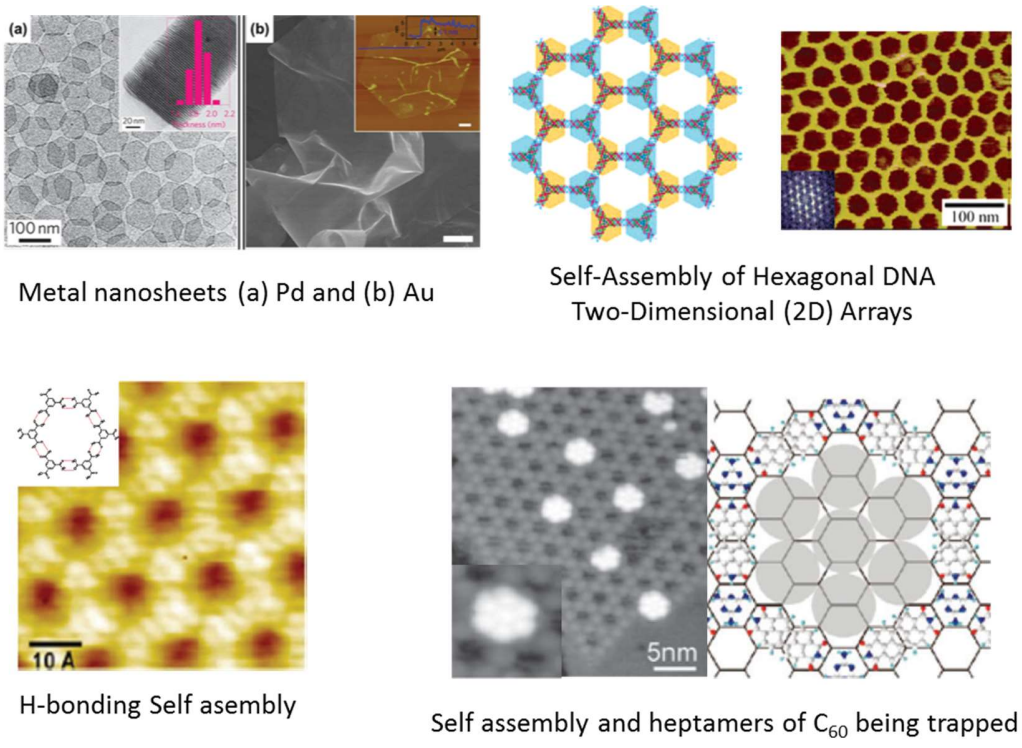

Figure 1.2.3 Different examples of self-assembly[81].

The free-standing ultrathin metallic nanosheets have been the research interest for number of applications in magnetism[89–91], catalysis[92], surface plasmonics resonance (SPR)[92] and as

theranostic agents[93]. The metals that have been fabricated to such nano assemblies are Rh[94], Ru[95], Pd[92,96], Au[97,98], Ag[99], Fe[100] and Cu[101]; even bimetallic systems like Pd@Ag[102], Pd@Au[93] or PtCu[103] are important to integrate tuning of SPR and improve photothermal stability. Being metallic and free coordination site, especially noble metal nanosheets are mostly useful for the catalysis; PtCu for ethanol hydrogenation, Rh for hydroformylation of 1-octene and hydrogenation of phenol[94]. The magnetic moments get enhanced from bulk crystal to single layers. The surfaces of single atom ferromagnetic layers' example Fe[100], have unsaturated coordination which directly leads to the improved spin and orbital moments. Hence integrating such ultrathin metallic films with other 2D materials would result in better spin torque devices, spin polarizers or spin filters.

1.2.4 Organic 2-D framework

The organic 2-D frameworks or better known as the covalent organic framework (COFs) are the recent interest of robust class of covalent materials. In 2005, Yaghi and his co-workers first synthesized the porous organic crystalline 2D materials[104]. The joining of simple organic molecules to a framework by using simple organic reaction, like boronate anhydride[104] or ester formation[105], borosilicate formation[106], nitrile cyclotrimerisation[107], Schiff base formation[108], hydrazone formation[109], led to new journey of COFs. Besides polymerization, porosity, structural regularity and inducing functionality[17,110] are the key factors for the development of such framework. The application side of the COFs can be broadly of three types: a) photo electric applications, b) gas storage, and c) catalysis.

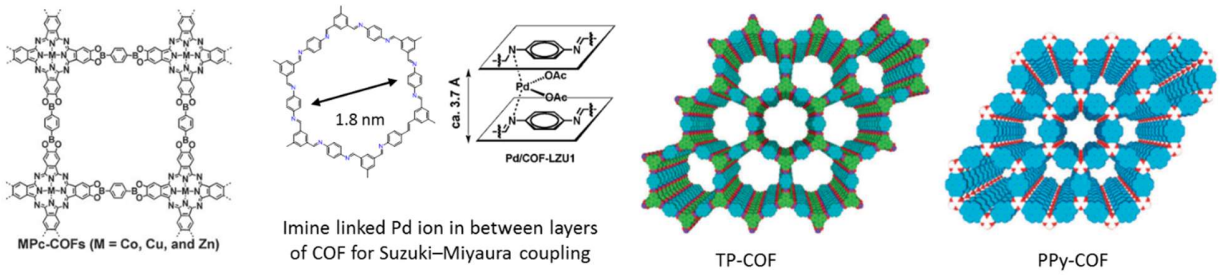

Figure 1.2.4 Different examples of COFs depending on their application[17,110].

Introduction of different moieties like pyrene[111,143], phthalocyanines[112–114], porphyrins[115–117] changed variety of photoconductive phenomenon in framework. As an example, TP-COF[111]

prepared by Jiang and co-workers is highly luminescent and harvests photons from ultraviolet to visible regions; in addition, it exhibits the p-type semiconductive[111] characters due to the eclipsed arrangement of triphenylene and pyrene units. COF features a remarkably large surface area and can be used for both gas adsorption and catalysis. Similar to zeolites, hybrids COFs can be heterogenous catalyst[118], although only two examples are known, performing Suzuki-Miyaura[108], Sonogashira[119], Heck or sequential one pot Heck-Sonogashira coupling reactions and enantioselective high-yielding Michael reactions[120]. On the other hand, gas adsorption[17,110] such as hydrogen, methane, ammonia and carbon dioxide has been reported.

1.3 Importance of Bottom-Up Approach

Since 2004, exfoliation of the bulk crystals was the key way to produce different 2-D layered materials ranging from graphene to transition metal dichalcogenides. Due to usefulness of single layer for better performance and efficiency of fabricated device[121], it is rather hard to produce large films of such kind. Instead building up from simple units is rather considerable approach for better quality and controlled growth for such minute single layered devices. It has been proved that chemical vapor deposition CVD generates better quality material than mechanically exfoliated films. CVD is one of the versatile techniques applied for bottom-up approach of many 2-D layered materials[122]. For the tuning of physical properties like the electrochemical and charge mobility[123], n-doping in graphene can be one of the cheap solutions. There are reports of boron[124], nitrogen[125] phosphorus[126] doping in graphene. All of these hetero atom dopings are carried out simultaneously with CVD nanosheet preparation. Similar observation was also seen with transition metal dichalcogenides[123]. By using CVD technique, metal mixed chalcogenides[122], MoS_2/WS_2 heterostructures[64] having ultrafast charge transfer have also been reported recently.

1.4 Coordination Nanosheet (CONASH)

In the light of considerable impact of 2-D layered material, there is a possibility that the framework can be built like as COFs, but instead of simple organic reaction to join two organic molecules, coordination chemistry can be used to coordinate metal and ligand moiety. This is advantageous to improvise 2-D COF to 2-D metal organic framework (MOF), as it gives more opportunities of catalytic site while considering the other applications unchanged. There is a room of full opportunities that can be considered for tuning the characteristics of the 2-D MOFs.

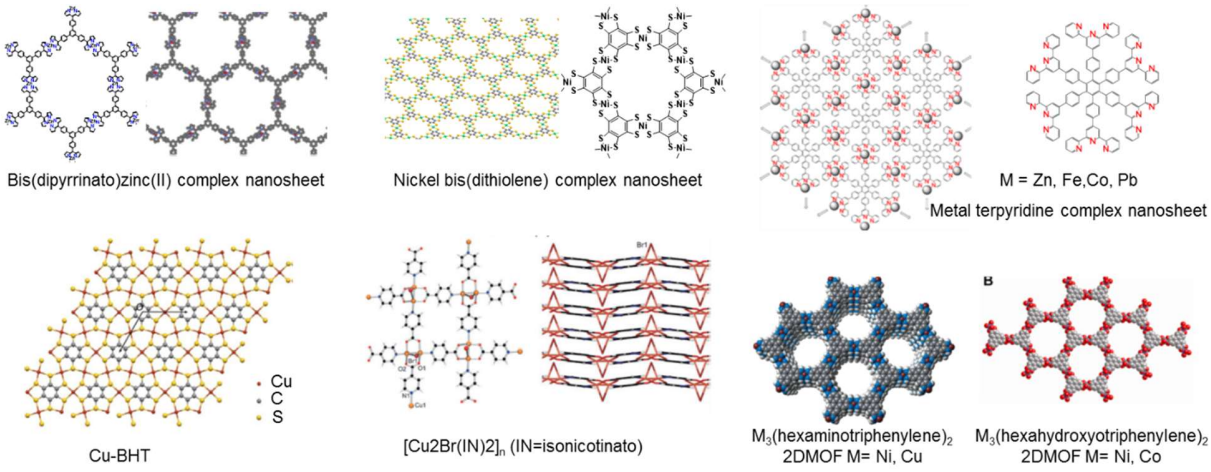

Figure 1.4.1 Different 2-D MOFs or coordination nanosheets (CONASHs)[127-135, 138, 144].

Comparing with other 2-D materials as described in previous sections, there is not much combinations except few metals and nonmetals but when we step into coordination nanosheets, we have whole range of coordination complexation including d-block and f-block metals with many combinations of p-block donor atoms. Moreover, this coordination happens easily at room temperature, hence higher elevated temperature as in case CVD may not be needed. Inducing functionality is easier through proper ligand design and metal choice. Dinca and co-workers have reported the nickel bis(hexaaminotriphennylene) complex nanosheets can electrochemically catalyze oxygen reduction reaction[127] and has semiconducting nature[128]; while its copper analogue sheet has ability to chemiresistive sensing[129,130] properties as well. The point to be noted here is the general procedure for synthesis of 2-D coordination polymer is via homogenous phase reaction containing both metal and ligand precursors. But Nishihara and coworkers showed interfacial

synthesis of 2-D polymers and explored interesting properties like change in oxidation states based on metal center of bis(terpyridine) Fe^{2+} or Co^{2+} complexes are functions of electrochromism[131], while replacing terpyridine moiety with bis(dipyrrinato)zinc(II) motif shows photoelectric conversion phenomenon[132]. In another case, change in the oxidation state based in the ligand center of nickel bis(dithiolene) complex nanosheet is a function of conductivity[133–135] up to 10^3 fold while changing from Ni to Co metal, efficient hydrogen evolution[136] from water has been reported by Marinescu and coworkers.

Interfacial reactions are more promising in order to make ordered structure. Polymers with large pores are often formed randomly in homogenous phase reactions resulting into an interpenetrated structure. For example, a layered planar polymeric structure might get interpenetrated with its own layers because of its large pore size forming 3-D structure and losses its planarity which might affect its physical properties thereby. Such an example is shown in Figure 1.4.2 b [137]. But it has been reported about the mono layer formation by interfacial synthesis which proves more efficient over the homogenous phase reaction.

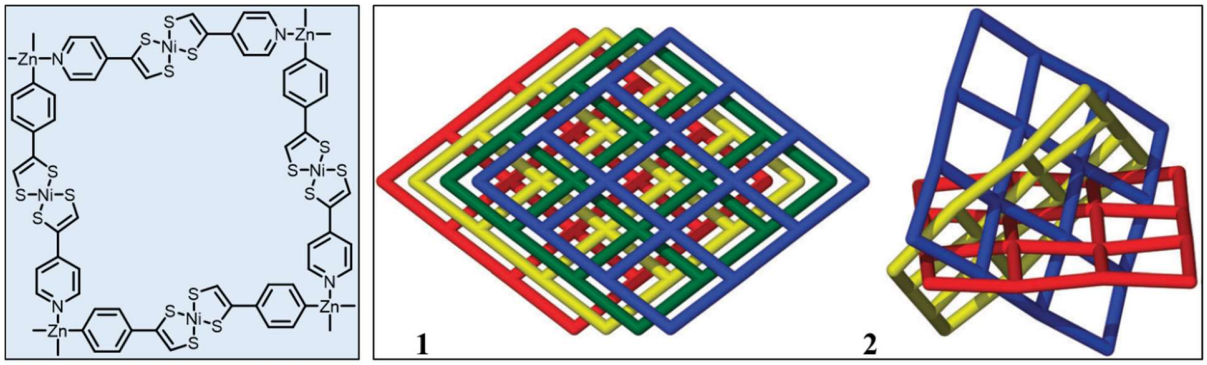

Figure 1.4.2 One unit of the polymer (left); illustration of 1 and 2, each color represents a discrete 2D net stacked polymer and the interpenetrated structure of the same unit by forming coordination (right)[137].

Band structure controls the general physical properties and in turn is a function of electron wave function of the distribution of atoms and molecules in the real space lattice which is directly guided by symmetry. Hence, symmetry is another important aspect of coordination complexation nanosheet. The symmetry of ligands and mode of coordination of metals play a vital role in defining the symmetry of the whole 2-D framework. For example, the symmetries of Cu-BHT[138]

complex nanosheet and nickel bis(dithiolene) complex nanosheet are completely different, in fact mode of coordination of Cu and Ni play a key role, although both the sheets diverge to a common ligand system. As a result of such difference in symmetry, the former shows a conductivity of 1580 S cm^{-1} while the later has a 160 S cm^{-1}. Hence, simple symmetry of ligand design and mode of coordination can alter intrinsic physical properties.

1.5 Aim of Research

1.5.1 Background

Different ligand systems have been the back bone of coordination chemistry with the vibrant support of the different metals of the Periodic table. Diamines, dithiols as non-innocent complexes and its wide class of derivatives have been known for their conductive properties. Previously, Kambe et al. synthesized nickel bis(dithiolene) complex 2-D layered nanosheet[135] having kagome lattice by simple coordination polymerization of benzenehexathiol (BHT) ligand with Ni^{2+} ions. Later, Liu and coworkers theoretically predicted the single layer of aforementioned nanosheet to have topological insulator (TI)[139] characteristics.

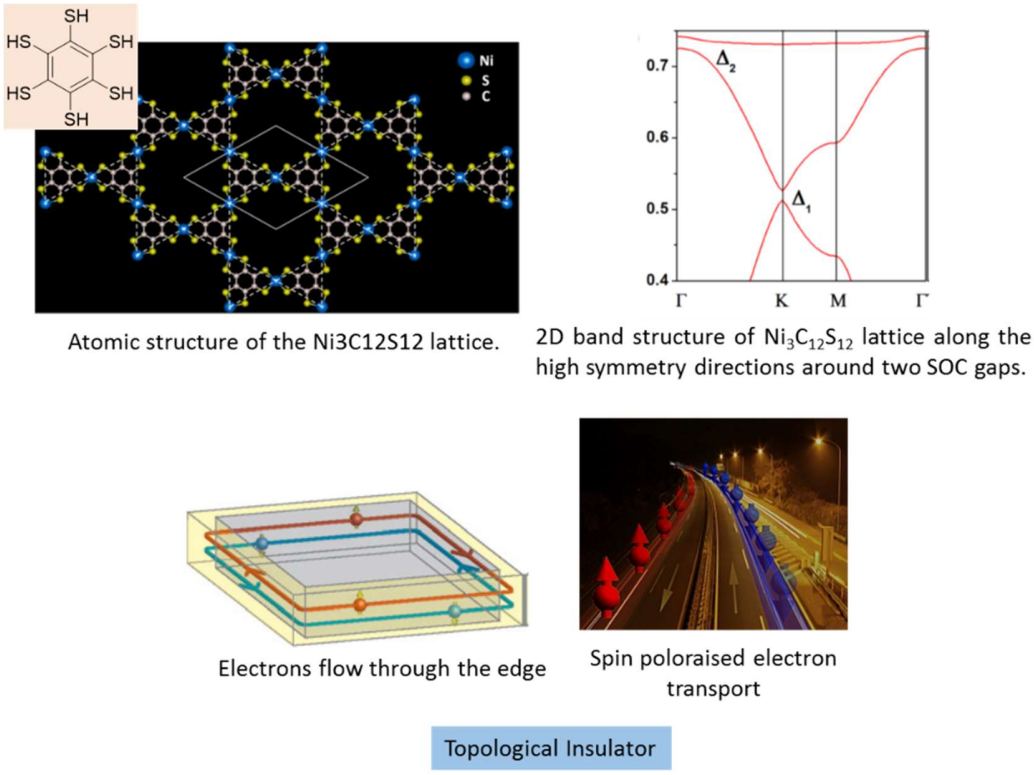

Figure 1.5.1 Prediction of TI characteristics of nickel bis(dithiolene) nanosheet[139].

TI being the new state of matter has interested researcher due to their intrinsic property of conduction over the edges and not by bulk conductivity unlike normal conductors. The bulk band structure resembles as an insulator, yet the intrinsic phenomenon underlies that the symmetry protected surface states[140] of such materials have a narrow gap and falls within the bulk gap. The

charge carriers are spin polarized i.e. the spin is locked at a right angle to their momentum (spin-momentum locking) hence there is no back scattering. It was also formulated that spin-orbit coupling (SOC) plays a vital role for the spin polarization as heavier elements increase the spin-orbit gap by splitting the topmost valence band so that SOC is strong enough to invert such insulating gap in case of TIs. Hence, building up such kind of 2-D coordinated layered material will be of much interest as for condensed matter physicists are concerned.

1.5.2 Problem Formulation

Taking a step further on replacing nickel by heavier metals of group 10 of nickel bis(dithiolene) the coordination complex nanosheet, it will be possible to increase SOC of the framework as the SOC increases down the group. Hence in my Ph.D. research, I focus at investigating on the synthetic strategies, electronic states and conductive behavior of heavier group 10 (Pd and Pt) metalladithiolene nanosheets due to the fact that heavier atoms have higher SOC. Additionally, it should be noted that their synthesis is highly challenging because the method to synthesize nickelladithiolene nanosheet by the reaction of Ni(II) ions and BHT cannot be simply applied because Pd(II) and Pt(II) system as they are easy to be reduced by thiols to their corresponding metallic state.

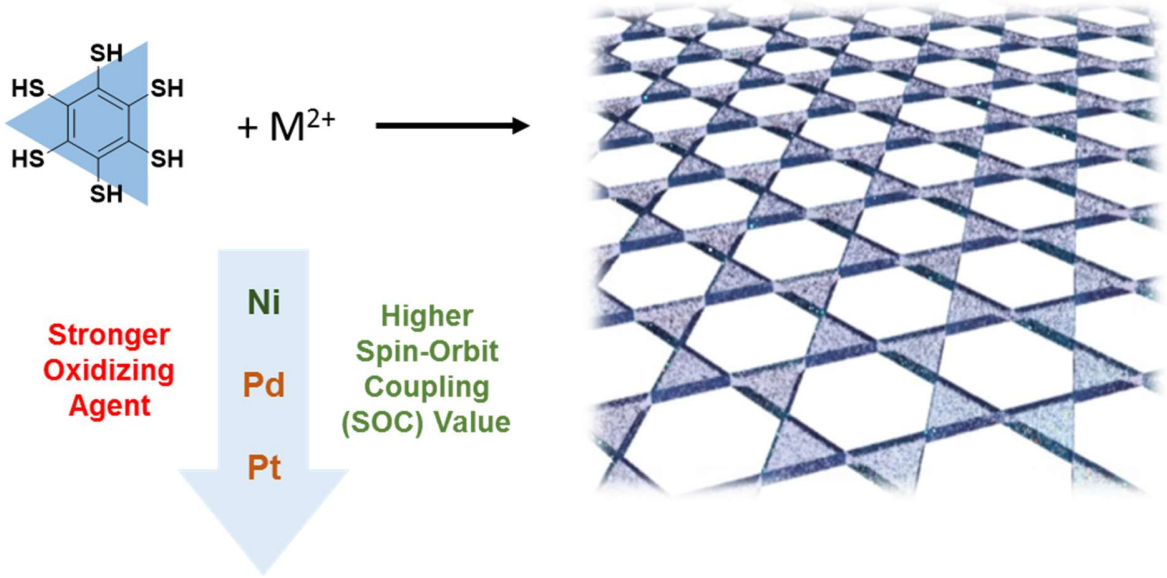

1.6 References:

1. Lovingood, D. D., Achey, R., Paravastu, A. K. & Strouse, G. F. Size- and site-dependent reconstruction in CdSe QDs Evidenced by ^{77}Se {^{1}H} CP-MAS NMR spectroscopy. *J. Am. Chem. Soc.* **132**, 3344–3354 (2010).

2. Lim, S. J., Zahid, M. U., Le, P., Ma, L., Entenberg, D., Harney, A. S., Condeelis, J. & Smith, A. M. Brightness-equalized quantum dots. *Nat. Commun.* **6**, 1–10 (2015).

3. Gong, X., Yang, Z., Walters, G., Comin, R., Ning, Z, Beauregard, E., Adinolfi, V., Voznyy, O. & Sargent, E. H. Highly efficient quantum dot near-infrared light-emitting diodes. *Nat. Photon.* **10**, 253–258 (2016).

4. Konstantatos, G., Badioli, M., Gaudreau, L., Osmond, J., Bernechea, M., Arquer, F. P. G., Gatti, F. & Koppens, F. H. L. Hybrid graphene–quantum dot phototransistors with ultrahigh gain. *Nat. Nanotech.* **7**, 363–368 (2012).

5. Lin, Y., Dimitrakopoulos, C., Jenkins, K. A., Farmer, D. B., Chiu, H.-Y., Grill, A. & Avouris, Ph. 100-GHz Transistors from wafer scale epitaxial graphene. *Science* **327** , 662 (2010).

6. Kan, E., Li, M., Hu, S., Xiao, C., Xiang, H. & Deng, K. Two-dimensional hexagonal transition-metal oxide for spintronics. *J. Phys. Chem . Lett.* 4, 1120-1125 (2013).

7. Mueller, T., Xia, F. & Avouris, P. Graphene photodetectors for high-speed optical communications. *Nat. Photon.* **4**, 297–301 (2010).

8. Bao, Q. & Loh, K. P. Graphene photonics, plasmonics, and broadband optoelectronic devices. *ACS Nano* **6**, 3677–3694 (2012).

9. Bonaccorso, F., Sun, Z., Hasan, T. & Ferrari, A. C. Graphene photonics and optoelectronics. *Nat. Photon.* **4**, 611–622 (2010).

10. Kroto, H. W. The stability of the fulerenes C_n, with n = 24,28,32,36,50,60 and 70. *Nature* **329**, 529–531 (1987).

11. Courtney, C. M., Goodman, S. M., Mcdaniel, J. A. & Madinger, N. E. Photoexcited quantum dots for killing multidrug-resistant bacteria. *Nat. Mater.* **15**, 529-535 (2016).

12. Sanchez-Valencia, J. R., Dienel1, T., Gro, O., Shorubalko, I., Mueller, A., Jansen, M., Amsharov, K., Ruffieux, P. & Fasel, R. Controlled synthesis of single-chirality carbon nanotubes. *Nature* **512**, 61–64 (2014).

13. Fromm, K. M. Coordination polymer networks with s-block metal ions. *Coord. Chem. Rev.* **252**, 856–885 (2008).

14. Welte, L., Calzolari, A., Di Felice, R., Zamora, F. & Gómez-Herrero, J. Highly conductive self-assembled nanoribbons of coordination polymers. *Nat. Nanotech.* **5**, 110–115 (2010).

15. Novoselov, K. S., Geim, A. K., Morozov, S. V., Jiang, D., Zhang, Y., Dubonos, S. V., Grigorieva, I. V. & Firsov, A. A. Electric field effect in atomically thin carbon films. *Science* **306**, 666–669 (2004).

16. Novoselov, K. S. & Geim, A. K. The rise of graphene. *Nat. Mater*. **6**, 183–191 (2007).

17. Ding, S.-Y. & Wang, W. Covalent organic frameworks (COFs): from design to applications. *Chem. Soc. Rev.* **42**, 548–568 (2013).

18. Hsieh, D., Qian, D., Wray, L., Xia, Y., Hor, Y. S., Cava, R. J. & Hasan, M. Z. A topological Dirac insulator in a quantum spin Hall phase. *Nature* **452**, 970–974 (2008).

19. Zhang, Y., Tan, Y., Stormer, H. L. & Kim, P. Experimental observation of the quantum Hall effect and Berry's phase in graphene. *Nature* **438**, 201–204 (2005).

20. Favron, A., Gaufrès, E., Fossard, F., Heureux, Anne-Laurence P.-L., Tang N. Y.-W., Lévesque, P. L., Loiseau, A., Leonelli, R., Francoeur, S. & Martel, R. Photooxidation and quantum confinement effects in exfoliated black phosphorus. *Nat. Mater.* **14**, 826-833 (2015).

21. Zhang, Y., Tang, T.-Ta, Girit, C., Hao, Z., Martin, M. C., Zettl, A., Crommie, M. F., Shen, Y. R. & Wang, F. Direct observation of a widely tunable bandgap in bilayer graphene. *Nature* **459**, 820–823 (2009).

22. Meric, I., Han, M. Y., Young, A. F., Ozyilmaz, B., Kim, P. & Shepard, K. L. Current saturation in zero-bandgap, top-gated graphene field-effect transistors. *Nat. Nanotech.* **3**, 654–659 (2008).

23. Novoselov, K. S., Geim, A. K., Morozov, S. V., Jiang, D., Katsnelson, M. I., Grigorieva, I. V., Dubonos, S. V. & Firsov, A. A. Two-dimensional gas of massless Dirac fermions in graphene. *Nature* **438**, 197–200 (2005).

24. Peimyoo, N., Li, J., Shang, J., Shen, X., Qiu, C., Xie, L., Huang, W. & Yu, T. Photocontrolled molecular structural transition and doping in graphene. *ACS Nano* **6**, 8878–8886 (2012).

25. Koehler, F. M., Jacobsen, A., Ensslin, K., Stampfer, C. & Stark, W. J. Selective chemical modification of graphene surfaces : distinction between single- and bilayer graphene. *Small* **6**, 1125–1130 (2010).

26. Functionalized, G., Jeon, E. K., Kang, D., Kim, G., Kim,B.-S., Kang, D. J. & Shin, H. S. Reversibly light-modulated Dirac point of graphene functionalized with spiropyran. *ACS Nano* **6**, 9207–9213 (2012).

27. Balog, R., Jørgensen, B., Nilsson, L., Andersen, M., Rienks, E., Bianchi, M., Fanetti, M., Lægsgaard, E., Baraldi, A., Lizzit, S., Sljivancanin, Z., Besenbacher, F., Hammer, B., Pedersen, T.G., Hofmann, P. & Hornekær, L. Bandgap opening in graphene induced by patterned hydrogen adsorption. *Nat. Mater.* **9**, 315–319 (2010).

28. Cai, J., Ruffieux, P., Jaafar, R., Bieri1, M., Braun, T., Blankenburg, S., Muoth, M., Seitsonen, A. P., Saleh, M., Feng, X., Müllen, K. & Fasel, R. Atomically precise bottom-up fabrication of graphene nanoribbons. *Nature* **466**, 470–3 (2010).

29. Tour, J. M. Top-down versus bottom-up fabrication of graphene-based electronics. *Chem. Mater.* **26**, 163–171 (2014).

30. Haley, M. M. Synthesis and properties of annulenic subunits of graphyne and graphdiyne nanoarchitectures. *Pure Appl. Chem.* **80**, 519–532 (2008).

31. Peng, Q., Dearden, A. K., Crean, J., Han, L., Liu, S., Wen, X. & De, S. New materials graphyne, graphdiyne, graphone and graphane : review of properties , synthesis , and application in nanotechnology. *Nanotechnol. Sci. Appl.* **7**, 1–29 (2014).

32. Feng, L. & Zhang, W. X. The structure and magnetism of graphone. *AIP Adv.* **2**, 042138 1-6 (2012).

33. Elias, D. C., Nair, R. R., Mohiuddin, T. M. G., Morozov, S. V., Blake, P., Halsall, M. P., Ferrari, A. C., Boukhvalov, D. W., Katsnelson, M. I., Geim, A. K. & Novoselov, K. S. Control of graphen's properties by reversible hydrogenation: evidence for graphane. *Science* **323**, 610-613 (2009).

34. Resta, A., Leoni, T., Barth, C., Ranguis, A., Becker, C., Bruhn, T., Vogt, P. & Lay, G. L. Atomic structures of silicene layers grown on Ag(111): scanning tunneling microscopy and noncontact atomic force microscopy observations. *Sci. Rep.* **3**, 2399 (2013).

35. Jose, D. & Datta, A. Structures and electronic properties of silicene: unlike graphene. *Acc. Chem. Res.* **47**(2), 593-602 (2014).

36. Feng, J., Wagner, S. R. & Zhang, P. Interfacial coupling and electronic structure of two-dimensional silicon grown on the Ag (111) surface at high temperature. *Nat. Publ. Gr.* 1–9 (2015).

37. Cahangirov, S., Topsakal, M., Aktu, E. & Ciraci, S. Two- and one-dimensional honeycomb structures of silicon and germanium. *Phys. Rev. Lett.* **102**, 236804, 1–4 (2009).

38. Ni, Z., Liu, Q, Tang, K., Zheng, Z., Zhou, J., Qin, R., Gao, Z. Yu, D. & Lu, J. Tunable bandgap in silicene and germanene. *Nano Lett.* **12**, 113–118 (2012).

39. Tao, L., Cinquanta, E., Chiappe, D., Grazianetti, C., Fanciulli, M., Dubey, M., Molle, A. & Akinwande, D. Silicene field-effect transistors operating at room temperature. *Nat. Nanotech.* **10**, 227–231 (2015).

40. Liu, C., Feng, W. & Yao, Y. Quantum spin Hall effect in silicene and two-dimensional germanium. *Phys. Rev. Lett.* **107**, 076802**,** 1–4 (2011).

41. An, X., Zhang Y., Liu, J. & Li, S. Quantum spin Hall effect induced by electric field in silicene. *Appl. Phys*. Lett. **102**, 043113 1–5 (2013).

42. Tahir, M. & Schwingenschlo, U. Valley polarized quantum Hall effect and topological insulator phase transitions in silicene. *Sci. Rep.* **3**, 1075, 1-5 (2013).

43. Ezawa, M. Quantum Hall Effects in Silicene. *J. Phys. Soc. Japan* **81**, 064705 1–6 (2012).

44. Liu, F., Liu, C., Wu, K. Yang, F. & Yao, Y. $d + id'$ Chiral superconductivity in bilayer silicene. *Phys. Rev. Lett.* **111**, 066804 1–5 (2013).

45. Xu, C., Luo, G., Liu, Q., Zheng, J., Zhang, Z., Nagase, S., Gao, Z. & Lu, J. Giant magnetoresistance in silicene nanoribbons. *Nanoscale* **4**, 3111–3117 (2012).

46. Dávila, M. E., Xian, L., Cahangirov, S., Rubio, A. & Lay, G. Le. Germanene : a novel two-dimensional germanium allotrope akin to graphene and silicene. *New J. Phys.* **16**, 095002 1-10, (2014).

47. Bianco, E., Butler, S., Jiang, S., Restrepo, O. D., Windl, W. & Goldberger, J. E. Stability and exfoliation of germanane : a germanium graphane analogue. *ACS Nano* **7**, 4414–4421 (2013).

48. Li, L., Yu, Y., Ye, G. J., Ge, Q., Ou, X., Feng, D., Chen, X. H. & Zhang, Y. Black phosphorus field-effect transistors. *Nat. Nanotechnol.* **9,** 372–377 (2014).

49. Brent, J. R., Savjani, N., Lewis, E. A., Haigh, S. J., Lewis, D. J. & O'Brien, P. Production of few-layer phosphorene by liquid exfoliation of black phosphorus. *Chem. Commun.* **50,** 13338–13341 (2014).

50. Tayari, V., Hemsworth, N., Fakih, I., Favron, A., Gaufres, E., Gervais, G., Martel, R. & Szkopek T. Two-dimensional magnetotransport in a black phosphorus naked quantum well. *Nat. Commun.* **6**, 7702 1–7 (2015).

51. Jia, Y., Xia, F. & Wang, H. Rediscovering black phosphorus as an anisotropic layered material for optoelectronics and electronics. *Nat. Commun.* **5,** 1–6 (2014).

52. Sun, J., Lee, H. W., Pasta, M., Yuan, H., Zheng, G., Sun, Y., Li, Y. & Cui, Y. A phosphorene–graphene hybrid material as a high-capacity anode for sodium-ion batteries. *Nat. Nanotech.* **10**, 980–985 (2015).

53. Mannix, A. J., Zhou, X. F., Kiraly, B., Wood, J. D., Alducin, D., Myers, B. D., Liu, X. & Fisher, B. L., Santiago, U., Guest, J. R., Yacaman, M. J., Ponce, A., Oganov, A. R., Hersam, M. C. & Guisinger, N. P. Synthesis of borophenes: anisotropic, two-dimensional boron poblymorphs. *Science* **350** , 1513-1516 (2013).

54. Zhu, F., Chen, W. J., Xu, Y., Gao, C. L., Guan, D. D., Liu, C. H., Qian, D., Zhang, S. C. & Jia, J. F. Epitaxial growth of two-dimensional stanene. *Nat. Mater.* **14**, 1020- 1026 (2015).

55. Xu, Y., Gan, Z. & Zhang, S. C. Enhanced thermoelectric performance and anomalous seebeck effects in topological insulators. *Phys. Rev. Lett.* **112**, 226801 1–5 (2014).

56. Wang, J., Xu, Y. & Zhang, S. Two-dimensional time-reversal-invariant topological superconductivity in a doped quantum spin-Hall insulator. *Phys. Rev. B* **90**, 054503, 1–5 (2014).

57. Tran, T. T., Bray, K., Ford, M. J., Toth, M. & Aharonovich, I. Quantum emission from hexagonal boron nitride monolayers. *Nat. Nanotech.* **11**, 37-41 (2016).

58. Woessner, A., Lundeberg, M. B., Gao, Y., Principi, A., González, P. A., Carrega, M., Watanabe, K., Taniguchi, T., Vignale, G., Polini, M., Hone, J., Hillenbrand, R. & Koppens, F. H. L. Highly confined low-loss plasmons in graphene–boron nitride heterostructures. *Nat. Mater.* **14**, 421–425 (2014).

59. Xu, X., Yao, W., Xiao, D. & Heinz, T. F. Spin and pseudospins in layered transition metal dichalcogenides. *Nat. Phys.* **10**, 343-350 (2014).

60. Schmidt, H., Wang, S., Chu, L. Toh, M., Kumar, R., Zhao, W., Neto, A. H. C., Martin, J., Adam, S., Özyilmaz, B. & Eda, G. Transport properties of monolayer MoS_2 grown by chemical vapor deposition. *Nano Lett.* **14**, 1909-1913 (2014).

61. Zeng, H., Dai, J., Yao, W., Xiao, D. & Cui, X. Valley polarization in MoS_2 monolayers by optical pumping. *Nat. Nanotech.* **7**, 490-493 (2012).

62. Ross, J. S., Klement, P., Jones, A. M., Ghimire, N. J., Yan, J., Mandrus, D. G., Taniguchi, T., Watanabe, K., Kitamura, K., Yao, W., Cobden, D. H. &Xu, X. Electrically tunable excitonic light-emitting diodes based on monolayer WSe_2 p–n junctions. *Nat. Nanotech.* **9**, 268–272 (2014).

63. Sun, L., Lin, J., Peng, J., Weng, J., Huang, Y. & Luo, Z. Preparation of few-layer bismuth selenide by liquid-phase-exfoliation and its optical absorption properties. *Sci. Rep.* **4**, 4794 (2014).

64. Huang, C., Wu, S., Sanchez, A. M., Peters, J. J. P., Beanland, R., Ross, J. S., Rivera, P., Yao, W., Cobden, D. H. & Xu, X. Lateral heterojunctions within monolayer $MoSe_2$ – WSe_2 semiconductors. *Nat. Mater.* **13**, 1096-1101 (2014).

65. Roy, A., Movva, H. C. P., Satpati, B., Kim, K., Dey, R., Rai, A., Pramanik, T., Guchhait, S., Tutuc, E. & Bannerjee, S. K. Structural and electrical properties of $MoTe_2$ and $MoSe_2$ grown by molecular beam epitaxy. *ACS Appl. Mater. Interfaces* **8**, 7396-7402 (2016).

66. Radisavljevic, B., Radenovic, A., Brivio, J., Giacometti, V. & Kis, A. Single-layer MoS_2 transistors. *Nat. Nanotech.* **6**, 147-150 (2011).

67. Wang, Q. H., Kalantar-zadeh, K., Kis, A., Coleman, J. N. & Strano, M. S. Electronics and optoelectronics of two-dimensional transition metal dichalcogenides. *Nat. Nanotech.* **7**, 699–712 (2012).

68. Mak, K. F., He, K., Shan, J. & Heinz, T. F. Control of valley polarization in monolayer MoS_2 by optical helicity. *Nature Nanotechnology* **7,** 494–498 (2012).

69. Feng, L., Fan, M., Wu, Y., Liu, Y. & Li, G. Metallic Co_9S_8 nanosheets grown on carbon cloth as efficient binder-free electrocatalysts for the hydrogen evolution reaction in neutral media. *J. Mater. Chem. A Mater. Energy Sustain.* **4**, 6860–6867 (2016).

70. Wang, L. & Sasaki, T. Titanium oxide nanosheets : graphene analogues with versatile functionalities. *Chem. Rev.* **114**, 9455-9486 (2014).

71. Ma, R., Takada, K., Fukuda, K., Iyi, N., Bando, Y. & Sasaki, T. Topochemical synthesis of monometallic (Co^{2+}-Co^{3+}) layered double hydroxide and its exfoliation into positively charged $Co(OH)_2$ nanosheets. *Angew. Chemie. Int. Ed.* **47**, 86–89 (2008).

72. Ma, B. R. & Sasaki, T. Nanosheets of oxides and hydroxides : ultimate 2D charge-bearing functional crystallites. *Adv. Mater.* **22**, 5082–5104 (2010).

73. Lee, K.-H., Lee, B.-I., You, J.-H. & Byeon, S.-H. Transparent Gd_2O_3 : Eu phosphor layer derived from exfoliated layered gadolinium hydroxide nanosheets. *Chem. Commun.* **46**, 1461–1463 (2010).

74. Yoon, Y. S., Lee, B. I., Lee, K. S., Im, G. H., Byeon, S. H., Lee, J. H. & Lee, I. S. Surface modification of exfoliated layered gadolinium hydroxide for the development of multimodal contrast agents for MRI and fluorescence imaging. *Adv. Funct. Mater.* **19**, 3375–3380 (2009).

75. Lee, B. I., Lee, K. S., Lee, J. H., Lee, I. S. & Byeon, S. H. Synthesis of colloidal aqueous suspensions of a layered gadolinium hydroxide: a potential MRI contrast agent. *Dalton Trans.* **14**, 2490–2495 (2009).

76. Naguib, M., Mashtalir, O., Carle, J., Presser, V., Lu, J., Hultman, L., Gogotsi, Y. & Barsoum, M. W. Two-dimensional transition metal carbides. *ACS Nano* **6**, 1322–1331 (2012).

77. Ghidiu, M., Lukatskaya, M. R., Zhao, M., Gogotsi, Y. & Barsoum, M. W. Conductive two-dimensional titanium carbide 'clay' with high volumetric capacitance. *Nature* **516**, 78-81 (2014).

78. Halim, J., Lukatskaya, M. R., Cook, K. M., Lu, J., Smith, C. R., Naslund, L. A., May, S. J., Hultman, L., Ggotsi, Y., Eklund, P. & Barsoum, M W. Transparent conductive two-dimensional titanium carbide epitaxial thin films. *Chem. Mater.* **26**, 2374-2381 (2014).

79. Gatti, R., MacLeod, J. M., Duffin, J. A. L., Moiseev, A. G., Perepichka, D. F. & Rosei, F. Substrate, molecular structure, and solvent effects in 2D self- assembly via hydrogen and halogen bonding. *J. Phys. Chem. C* **118**, 25505-25516 (2014).

80. Wieghold, S., Li, J., Simon, P., Krause, M., Avlasevich, Y., Li, C., Garrido, J. A., Heiz, U., Samori, P., Mullen, K., Esch, F., Barth, J. V. & Palma, C. A. Photoresponse of supramolecular self-assembled networks on graphene–diamond interfaces. *Nat. Commun.* **7**, 10700 1–8 (2016).

81. Kudernac, T., Lei, S., Elemans, J. A. A. W. & Feyter, S. De. Two-dimensional supramolecular self-assembly : nanoporous networks on surfaces. *Chem. Soc. Rev.* **38**, 402–421 (2009).

82. Lit, J. V. D., Marsman, J. L., Koster, R. S., Jacobse,P. H., Hartog, S. A. D., Vanmaekelbergh, D., Gebbink, J. M. K., Filion, L. & Swart, I. Modeling the self-assembly of organic molecules in 2D molecular layers with different structures. *J. Phys. Chem. C* **120**, 318-323 (2016).

83. Tuan, S., Pham, A. & Stöhr, M. Self-assembly of pyrene derivatives on Au(111): substituent effects on intermolecular interactions. *Chem. Commun.* **50**, 14089–14092 (2014).

84. Schull, G., Douillard, L., Debuisschert, C. F. & Charra, F. Single-molecule dynamics in a self-assembled 2D molecular sieve. *Nano Lett.* **6**, 1360–1363 (2006).

85. Yan, H., Park, S. H., Finkelstein, G., Reif, J. H. & Labean, T. H. DNA-templated self-assembly of protein arrays and highly conductive nanowires. *Science* **301**, 1882-1884 (2003).

86. He, Y., Chen, Y., Liu, h., Ribbe, A. E. & Mao, C. Self-assembly of hexagonal DNA two-dimensional (2D) arays. *J. Am. Chem. Soc.* **127**, 12202–12203 (2005).

87. Wintjes, N., Bonifazi, D., Cheng, F., Kiebele, A., Stohr, M., Jung, T., Spillmann, H. & Diederich, F. A supramolecular multiposition rotary device. *Angew. Chemie. Int. Ed.* **46**, 4089–4092 (2007).

88. Stöhr, M., Wahl, M., Spillmann, H., Gade, L. H. & Jung, T. A. Lateral manipulation for the positioning of molecular guests within the confinements of a highly stable self-assembled organic surface network. *Small* **3**, 1336–1340 (2007).

89. Bruno, P. Tight-binding approach to the orbital magnetic moment and magnetocrystalline aisotropy of transition-metal monolayers. *Phys. Rev. B* **39**, 865–868 (1989).

90. Qian, D., Jin, X. F., Barthel, J., Klaua, M. & Kirschner, J. Spin-density wave in ultrathin Fe films on Cu(100). *Phys. Rev. Lett.* **87**, 227204 1-4 (2001).

91. Hjortstam, O., Trygg, J., Wills, J., Johansson, B. & Eriksson, O. Calculated spin and orbital moments in the surfaces of the 3d metals Fe, Co, and Ni and their overlayers on Cu(001). *Phys. Rev. B* **53**, 9204–9213 (1996).

92. Huang, X.,Tang, S., Mu, X., Dai, Y., Chen, G., Zhou, Z., Ruan, F., Yang, Z. & Zheng, N. Freestanding palladium nanosheets with plasmonic and catalytic properties. *Nat. Nanotech.* **6**, 28–32 (2011).

93. Chen, M., Tang, S., Guo, Z., Wang, X., Mo, S., Huang, X., Liu, G. & Zheng, N. Core-shell Pd@Au nanoplates as theranostic agents for in-vivo photoacoustic imaging, CT imaging, and photothermal therapy. *Adv. Mater.* **26**, 8210–8216 (2014).

94. Duan, H., Yan, N., Yu, R., Chang, C. R., Zhou, G., Hu, H. S., Rong, H., Niu, Z., Mao, J., Asakura, H., Tanaka, T., Dyson, P. J., Li, J. & Li, Y. Ultrathin rhodium nanosheets. *Nat. Commun.* **5**, 3093 1-8 (2014).

95. Yin, A. X., Liu, W. C., Ke, J., Zhu, W., Gu, J., Zhang, Y. W. & Yan, C. H. Ru nanocrystals with shape-dependent surface-enhanced raman spectra and catalytic properties: Controlled synthesis and DFT calculations. *J. Am. Chem. Soc.* **134**, 20479–20489 (2012).

96. Yin, X., Liu, X., Pan, Y., Walsh, K. A. & Yang, H. Hanoi tower-like multilayered ultrathin palladium nanosheets. *Nano Lett.* **14**, 7188-7194 (2014).

97. Huang, X., Li, S., Huang, Y., Wu, S., Zhou, X., Li, S., Gan, C. L., Boey, F., Mirkin, C. A. & Zhang, H. Synthesis of hexagonal close-packed gold nanostructures. *Nat. Commun.* **2**, 292 1-6 (2011).

98. Niu, J., Wang, D., Qin, H., Xiong, X., Tan, P., Li, Y., Lu, X., Wu, J., Zhang, T., Ni, W. & Jin, J. Novel polymer-free iridescent lamellar hydrogel for two-dimensional confined growth of ultrathin gold membranes. *Nat. Commun.* **5**, 3313 1-7 (2014).

99. Zhang, Q., Hu, Y., Guo, S., Goebl, J. & Yin, Y. Seeded growth of uniform Ag nanoplates with high aspect ratio and widely tunable surface plasmon bands. *Nano Lett.* **10**, 5037–5042 (2010).

100. Zhao, J., Deng, Q., Bachmatiuk, A., Sandeep, G., Popov, A., Ecckert, J. & Rummeli, M. H. Free-standing single-atom-thick iron membranes suspended in graphene pores. *Science* **343**

, 1228-1232 (2014).

101. Wu, Z., Li, Y., Liu, J., Lu, Z., Zhang, H. & Yang, B. Colloidal self-assembly of catalytic copper nanoclusters into ultrathin ribbons. *Angew. Chemie. Int. Ed.* **53**, 12196–12200 (2014).

102. Huang, X., Tang, S., Liu, B., Ren, B. & Zheng, N. Enhancing the photothermal stability of plasmonic metal nanoplates by a core-shell architecture. *Adv. Mater.* **23**, 3420–3425 (2011).

103. Saleem, F., Zhang, Z., Xu, B., Xu, X., He, P. & Wang, X. Ultrathin Pt − Cu nanosheets and nanocones. *J. Am. Chem. Soc.* **135**, 18304-18307 (2013).

104. Ockwig, N. W., Cote, A. P., Keeffe, M. O., Matzger, A. J. & Yaghi, O. M. Porous , crystalline , covalent organic frameworks. *Science* **310**, 1166–1171 (2005).

105. Spitler, E. L. & Dichtel, W. R. Lewis acid-catalysed formation of two-dimensional phthalocyanine covalent organic frameworks. *Nat. Chem.* **2**, 672–677 (2010).

106. Hunt, J. R., Doonan, C. J., LeVangie, J. D., Côté, A. P. & Yaghi, O. M. Reticular synthesis of covalent organic borosilicate frameworks. *J. Am. Chem. Soc.* **130**, 11872–11873 (2008).

107. Kuhn, P., Antonietti, M. & Thomas, A. Porous, covalent triazine-based frameworks prepared by ionothermal synthesis. *Angew. Chemie. Int. Ed.* **47**, 3450–3453 (2008).

108. Ding, S.-Y., Gao, J., Wang, Q., Zhang, Y., Song, W. G., Su, C. Y. & Wang, W. Construction of covalent organic framework for catalysis: Pd/COF-LZU1 in Suzuki-Miyaura coupling reaction. *J. Am. Chem. Soc.* **133**, 19816–19822 (2011).

109. Uribe-Romo, F. J., Doonan, C. J., Furukawa, H., Oisaki, K. & Yaghi, O. M. Crystalline covalent organic frameworks with hydrazone linkages. *J. Am. Chem. Soc.* **133**, 11478–11481 (2011).

110. Feng, X., Ding, X. & Jiang, D. Covalent organic frameworks. *Chem. Soc. Rev.* **41**, 6010–22 (2012).

111. Wan, S., Guo, J., Kim, J., Ihee, H. & Jiang, D. A belt-shaped, blue luminescent, and semiconducting covalent organic framework. *Angew. Chemie. Int. Ed.* **47**, 8826–8830 (2008).

112. Ding, X., Guo, J., Feng, X., Honsho, Y., Guo, J., Seki, S., Maitarad, P., Saeki, A., Nagase, S. & Jiang, D. Synthesis of metallophthalocyanine covalent organic frameworks that exhibit high carrier mobility and photoconductivity. *Angew. Chemie. Int. Ed.* **50**, 1289–1293 (2011).

113. Spitler, E. L., Colson, J. W., Uribe-Romo, F. J., Woll, A. R., Giovino, M. R., Saldivar, A. & Dichtel, W. R. Lattice expansion of highly oriented 2D phthalocyanine covalent organic framework films. *Angew. Chemie. Int. Ed.* **51**, 2623–2627 (2012).

114. Ding, X., chen, L., Honsho, Y., Feng, X., Saengsawang, O., Guo, J., Saeki, A., Seki, S., Irle, S., Nagase, S., Parasuk, V. & Jiang, D. An n-channel two-dimensional covalent organic framework. *J. Am. Chem. Soc.* **133**, 14510–14513 (2011).

115. Feng, X., Liu, L., Honsho, Y., Saeki, A., Seki, S., Irle, S., Dong, Y, Nagai, A. & Jiang, D. High-rate charge-carrier transport in porphyrin covalent organic frameworks: Switching from hole to electron to ambipolar conduction. *Angew. Chemie. Int. Ed.* **51**, 2618–2622 (2012).

116. Wan, S., Gandara, F., Asano, A., Furukawa, H., Saeki, A., Dey, S. K., Liao, L., Ambrogio, M. W., Botros, Y. Y., Duan, X., Seki, S., Stoddart, J, F. & Yaghi, O, M. Covalent organic frameworks with high charge carrier mobility. *Chem. Mater.* **23**, 4094–4097 (2011).

117. Feng, X., Chen, L., Dong, Y. & Jiang, D. Porphyrin-based two-dimensional covalent organic frameworks: synchronized synthetic control of macroscopic structures and pore parameters. *Chem. Commun.* **47**, 1979–1981 (2011).

118. Dogru, M., Sonnauer, A., Zimdars, S., Doblinger, M., knochel, P. & Bein, T. Facile synthesis of a mesoporous benzothiadiazole-COF based on a transesterification process. *CrystEngComm* **15,** 1500–1502 (2013).

119. Pachfule, P., Panda, M. K., Kandambeth, S., Shivaprasad, S. M., Diaz, D. D. & Banerjee, R. Multifunctional and robust covalent organic framework–nanoparticle hybrids. *J. Mater. Chem. A* **2**, 7944–7952 (2014).

120. Xu, H. & Gao, J. Stable , crystalline , porous , covalent organic frameworks as a platform for chiral organocatalysts. *Nat. Chem.* **7**, 1–50 (2015).

121. Zhang, Y., Chang, T. R., Zhou, B., Cui, Y. T., Yan, H., Liu, Z., Schmitt, F., Lee, J., Moore, R., Chen, Y., Lin, H., Jeng, H. T., Mo, S. K., Hussain, Z., Bansil, A. & Shen, Z. X. Direct observation of the transition from indirect to direct bandgap in atomically thin epitaxial $MoSe_2$. *Nat. Nanotech.* **9**, 111–115 (2014).

122. Klee, V., Preciado, E., Barroso, D., Nguyen, A. E., Lee, C., Erickson, K. J., Triplett, M., Davis, B., Lu, I. H., Bobek, S., Mckinley, J., Martinez, J. P., Mann, J., Talin, A. A., Bartels, L. & Leonard, F. Superlinear composition-dependent photocurrent in CVD-grown monolayer $MoS_{2(1-x)}Se_{2x}$ Alloy Devices. *Nano Lett.* **15**, 2612-2619 (2015).

123. Yang, L., Majumdar, K., Liu, H., Du, Y., Wu, H., Hatzistergos, M., Hung, P. Y., Tieckelmann, R., Tsai, W., Hobbs, C. &Ye, P. D. Chloride molecular doping technique on 2D materials : WS_2 and MoS_2. *Nano Lett.* **14**, 6275-6280 (2014).

124. Wu, T., Shen, H., Sun, L., Cheng, B., Liu, B. & Shen, J. Nitrogen and boron doped monolayer graphene by chemical vapor deposition using polystyrene , urea and boric acid. *New J. Chem.* **36**, 1385–1391 (2012).

125. Bekyarova, E., Itkis, M. E., Ramesh, P., Berger, C., Sprinkle, M., Heer, W. A. D. & Haddon, R. C. Chemical modification of epitaxial graphene : spontaneous grafting of aryl groups. *J. Am. Chem. Soc.* **131**, 1336–1337 (2009).

126. Li, R., Wei, Z., Gou, X. & Xu, W. Phosphorus-doped graphene nanosheets as efficient metal-free oxygen reduction electrocatalysts. *RSC Advances* **3**, 9978–9984 (2013).

127. Miner, E. M., Fukushima, T., Sheberla, D., Sun, L., Surendranath, Y. & Dinca, M. Electrochemical oxygen reduction catalysed by Ni_3(hexaiminotriphenylene)$_2$. *Nat.*

Commun. **7**, 10942 1-7 (2016).

128. Sheberla, D., Sun, L., Blood-Forsythe, M. A., Er, S., Wade, C. R., Brozek, C. K., Aspuru-Guzik, A. & Dinca, M. High electrical conductivity in Ni_3(2,3,6,7,10,11-hexaiminotriphenylene)$_2$, a semiconducting metal-organic graphene analogue. *J. Am. Chem. Soc.* **136**, 8859–8862 (2014).

129. Campbell, M. G., Liu, S. F., Swager, T. M. & Dinca, M. Chemiresistive sensor arrays from conductive 2D metal-organic frameworks. *J. Am. Chem. Soc.* **137**, 13780–13783 (2015).

130. Campbell, M. G., Sheberla, D., Liu, S. F., Swager, T. M. & Dinca, M. Cu_3(hexaiminotriphenylene)$_2$: An electrically conductive 2D metal-organic framework for chemiresistive sensing. *Angew. Chemie. Int. Ed.* **54**, 4349–4352 (2015).

131. Takada, K., Sakamoto, R., Yi, S. T., Katagiri, S., Kambe, T. & Nishihara, H. Electrochromic bis(terpyridine)metal complex nanosheets. *J. Am. Chem. Soc.* **137**, 4681–4689 (2015).

132. Sakamoto, R., Hoshiko, K., Liu, Q., Yagi, T., Nagayama, T., Kusaka, S., Tsuchiya, M., Kitagawa, Y., Wong, W. Y. & Nishihara, H. A photofunctional bottom-up bis(dipyrrinato)zinc(II) complex nanosheet. *Nat. Commun.* **6**, 6713 1-9 (2015).

133. Kambe, T., Sakamoto, R., Kusamoto, T., Pal, T., Fukui, N., Hoshiko, K., Shimojima, T., Wang, Z., Hirahara, T., Ishizaka, K., Hasegawa, S., Liu, F. & Nishihara, H. Redox control and high conductivity of nickel bis(dithiolene) complex π-nanosheet: A potential organic two-dimensional topological insulator. *J. Am. Chem. Soc.* **136**, 14357–14360 (2014).

134. Hoshiko, K., Kambe, T., Sakamoto, R., Takada, K. & Nishihara, H. Fabrication of dense and multilayered films of a nickel bis(dithiolene) nanosheet by means of the Langmuir-Schäfer method. *Chem.Lett.* **43**, 252–253 (2014).

135. Kambe, T., Sakamoto, R., Hoshiko, K., Takada, K., Miyachi, M., Ryu, J. H., Sasaki, S., Kim, J., Nakazato, K., Takata, M. & Nishihara, H. π-Conjugated nickel bis(dithiolene) complex nanosheet. *J. Am. Chem. Soc.* **135**, 2462–2465 (2013).

136. Clough, A. J., Yoo, J. W., Mecklenburg, M. H. & Marinescu, S. C. Two-dimensional metal-organic surfaces for efficient hydrogen evolution from water. *J. Am. Chem. Soc.* **137**, 118–121 (2015).

137. Faust, T. B., Usov, P. M., D'Alessandro, D. M. & Kepert, C. J. Highly unusual interpenetration isomers of electroactive nickel bis(dithiolene) coordination frameworks. *Chem. Commun.* **50**, 12772–4 (2014).

138. Huang, X., Sheng, P., Tu, Z., Zhang, F., Wang, J., Geng, H., Zou, Y., Di, C. A., Yi, Y., Sun, Y., Xu, W. & Zhu, D. A two-dimensional π-d conjugated coordination polymer with extremely high electrical conductivity and ambipolar transport behaviour. *Nat. Commun.* **6**, 7408 1-8 (2015).

139. Wang, Z., Su, N. & Liu, F. T. Prediction of 2D organic topological insulator. *Nano Lett.* **13**, 2842-2845 (2013).

140. Hasan, M. Z. & Kane, C. L. Colloquium: Topological insulators. *Rev. Mod. Phys.* **82**, 3045–

3067 (2010).

141. Li, B. W., Osada, M., Ozawa, T. C., Ebina, Y., Akatsuka, K., Ma, R., Funakubo, H., and Sasaki, T. Engineered interfaces of artificial perovskite oxide superlattices via nanosheet deposition process. *ACS Nano* **4**, 6673–6680 (2010).

142. Abellán, G., Gastaldo, C. M., Ribera, A., and Coronado, E. Hybrid materials based on magnetic layered double hydroxides: a molecular perspective. *Acc. Chem. Res.* **48**, 1601−1611 (2015).

143. Wan, S., Guo, J., Kim, J., Ihee, H., and Jiang, D. A photoconductive covalent organic framework: self-condensed arene cubes composed of eclipsed 2D polypyrene sheets for photocurrent generation. *Angew. Chem.* **121**, 5547-5550 (2009).

144. Amo-Ochoa, P., Welte, L., Prieto, R.G., Miguel, P. J. S., Gómez-García, C. J., Mateo-Martí, E., Delgado, S., Gómez-Herrerob, J., and Zamora, F. Single layers of a multifunctional laminar Cu(I,II) coordination polymer. *Chem. Commun.* **46**, 3262–3264, (2010).

Chapter 2

π-Conjugated Palladium Bis(dithiolene) (PdDT) Coordination Nanosheets

2.1 Introduction

Research in 2-D coordination nanosheet (CONASH), or rather organic nanosheet, is now intensifying due to its versatility in tuning its properties over the whole range of periodic table by different combination of metals and strategic design of ligands forming isostructural inorganic lattices in ambient temperatures but also with specific optical-electronic properties. Previously, coordination polymerization of benenehexathiol (BHT) ligand with Ni^{2+} ions resulted in infinite 2-D layered multinucleated sheet[1,2]. Because of the increase in spin-orbit coupling (SOC), I attempt a step further by utilizing the noble metal palladium, (having higher SOC value than nickel), as a candidate for CONASH. Noble metals are known for their positive reduction potentials and remain a challenge of using them with non-innocent hexathiol ligand system[3], for the fabrication of nanosheets. The use of interfacial reaction has proved to be useful for highly ordered, crystalline, layered material synthesis unlike the generation of amorphous material by monophasic reaction. In this work, I report the synthetic strategies and characterization of palladium bis(dithiolene) complex nanosheets (**PdDT**).

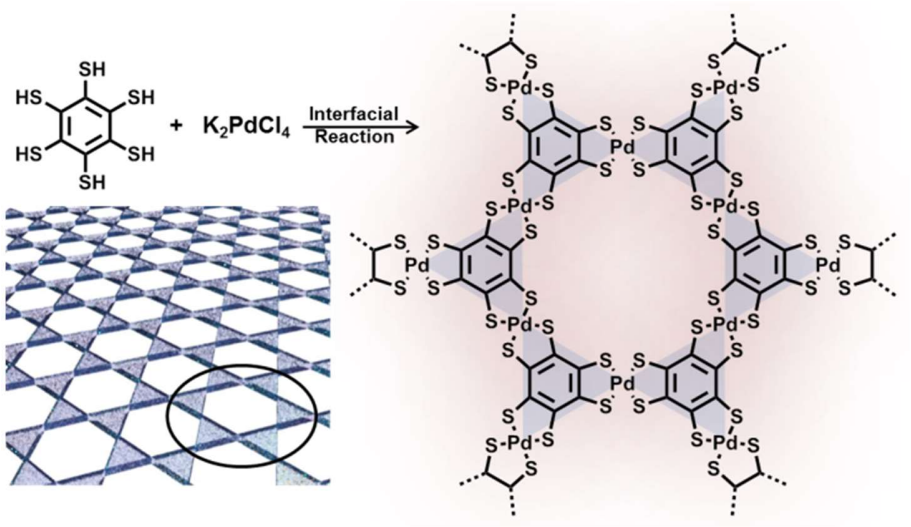

Scheme 2. Schematic illustration of palladium bis(dithiolene) nanosheet (**PdDT**).

2.2 Liquid-Liquid Interfacial Synthesis of Palladium Bis(dithiolene) (PdDT) CONASH

The pristine surface can be a mediating ground for reactions. We can exploit this kind of surfaces for the directional growth of the framework. In case of homogenous phase reaction, the framework will get intertwined as it lacks in directionality[11]. The framework being planar, the growth directionality should be directed in x-y plane only. Out of solid, liquid, and gaseous medium reactions, liquid and gaseous phase reactions are more fast and controlled reactions compared to solids. The layering of two almost immiscible pair of liquids makes certain measured common phase. To understand this, for example, for water and CH_2Cl_2 system, which forms an azeotrope mixture and solubility of CH_2Cl_2 in water being 17.5g/L at 25˚C, when layered will always form a very thin layer where both water and CH_2Cl_2 are miscible and is fixed depending on the volumes of the pair of liquids. This can be a suitable site of reaction which will add the directionality to the growth of the framework[4].

2.2.1 Synthesis of PdDT1

To synthesize **PdDT**, I employed the same approach similar to the case multilayer stacked nickel bis(dithiolene) CONASH or **NiDT**, which is a liquid-liquid interfacial reaction resulting to a high purity and larger domain of layered sheets. K_2PdCl_4 and NaBr in an aqueous phase and benzenehexathiole (BHT) in an organic phase (dichloromethane) were layered in argon atmosphere. NaBr was added to supply counter cation for the anionic form of **PdDT**, $[PdS_4]^-$ motif.

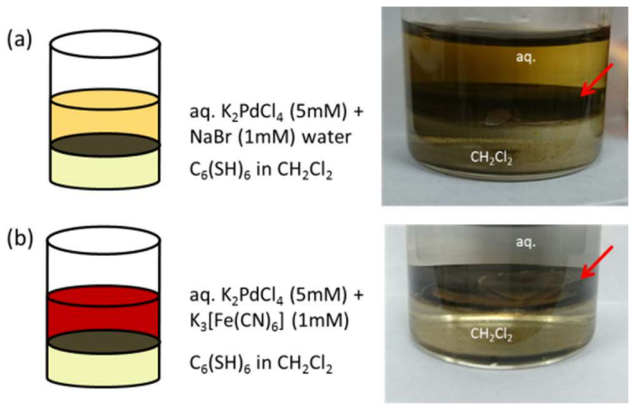

Figure 2.2.1 Fabrication of **micro-PdDT**. Both (a) and (b) illustrate liquid-liquid interfacial reaction and photography represent **1** and **2** (red arrow) at the interface, respectively.

After letting the two-phase solution standing overnight, a thin lustrous black film was formed at the interphase as shown in Figure 2.2.1a. Thickness of the **PdDT** film is around 2 - 3 μm and the film is referred to as **PdDT1**. The schematic equation is given in eq (i).

$$1.5\,[PdCl_4]^{2-} + C_6(SH)_6 \longrightarrow (C_6S_6Pd_{1.5})_n^{0/-1} + Pd^0 + 6\,HCl \quad \text{.....eq (i)}$$

BHT **PdDT** nanosheet

2.2.2 Results and Discussion of PdDT1

TEM measurement of **PdDT1** displays a sheet material with some nm-scale grains (Figure 2.2.2 a,b). Powder XRD of **PdDT1** shows several peaks characteristic of Pd(0) (Figure 2.2.2 c), implying that the observed grains are of metallic Pd(0)[9]. The TEM and XRD data reveal the distribution of these grains of metallic Pd in the range of 3-5 nm diameter (Figure 2.2.2 b) which can be called as palladium nanoparticles PdNPs. The plausible reaction schemes are shown in Figure 2.3.1. This implies that the non-innocent BHT in dichloromethane has less positive potential than the Pd^{2+}/Pd^0 couple and acts as a reducing agent.

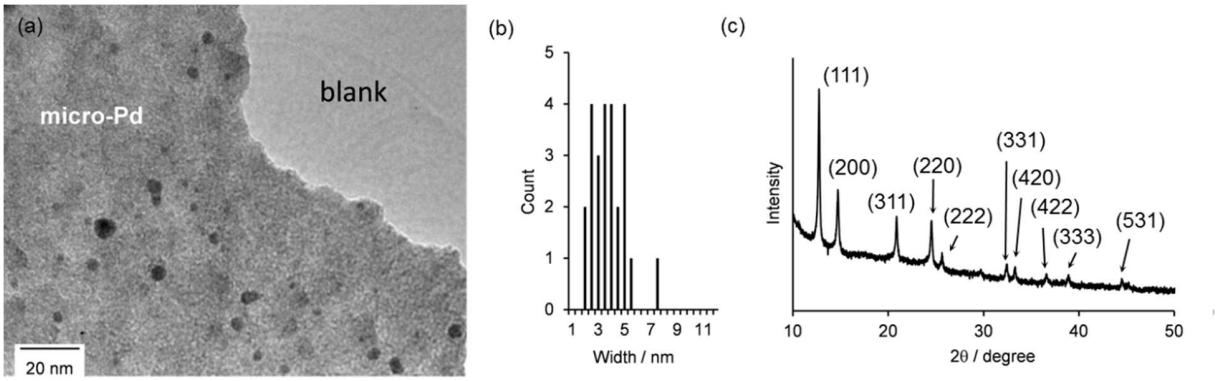

Figure 2.2.2 (a) TEM image showing **PdDT1** sheet having black particles of Pd(0), (b) distribution of PdNPs as observed in (a). (c) Powder XRD data of (a). Observed peaks are corresponding to Pd(0) metal.

2.3 Liquid-Liquid Interfacial Synthesis of Nanoparticles Free PdDT

To prevent the formation of PdNPs, I introduced a layer of oxidizing agent, potassium ferricyanide ($K_3[Fe(CN)_6]$) in the aqueous layer to act as redox buffer which will prevent reduction of Pd^{2+} to Pd(0) as given in eq(ii), before starting the liquid-liquid interfacial reaction as shown in Figure 2.3. The amount of $K_3[Fe(CN)_6]$ strongly affects the film formation; addition of 1 mM $K_3[Fe(CN)_6]$ resulted in a formation of a black nanosheet with metallic luster, whereas 2 mM of $K_3[Fe(CN)_6]$ gave a pale blue material as shown in Figure 2.3. Further addition of $K_3[Fe(CN)_6]$ formed amorphous substance which does not have any sheet like morphology. The reaction condition A was found to be have sheet like morphology, so that further characterization was carried out with it and the sheet is called as **PdDT2**.

$$1.5\ K_2PdCl_4 + 0.3\ K_3[Fe(CN)]_6 + C_6(SH)_6 \longrightarrow (C_6S_6Pd_{1.5})_n^{0/-1} + K_2[Fe(CN)]_6 + K^+ + 6Cl^- + 6H^+ \quad \text{eq (ii)}$$

BHT **PdDT** nanosheet

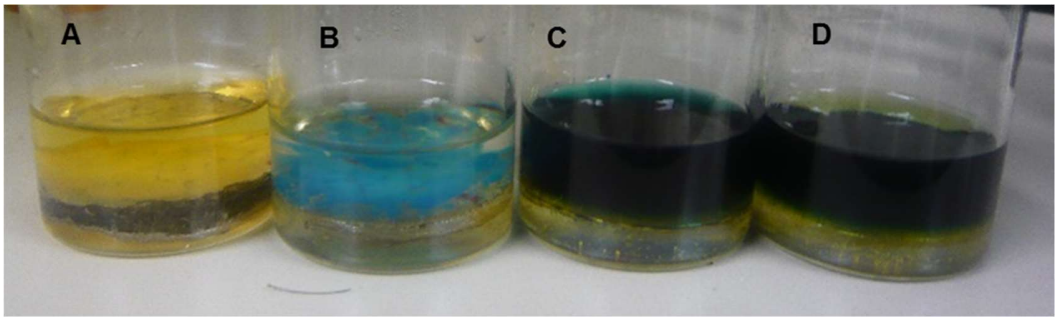

Figure 2.3 Photograph focusing on the water-dichloromethane interfaces with $K_3[Fe(CN)_6]$ in the aqueous layers. The concentrations of $K_3[Fe(CN)_6]$ are 1 mM, 5 mM, 10 mM, and 20 mM in A, B, C, D, respectively.

2.4 TEM and Selected Area Diffraction of PdDT2

Transmission electron microscopy (TEM) displayed a sheet like morphology of **PdDT2** in Figure 2.4 a. It is noteworthy that Pd(0) nanoparticles were not seen, which proves that $K_3[Fe(CN_6)]$ acts as an oxidizing agent and a redox buffer. In Figure 2.4 b, the edge has a stair like morphology which proves that it has a layered structure. Furthermore, selected area electron diffraction (SAED) showed a hexagonal diffraction pattern Figures 2.4 c, implying the skeleton of the framework has a hexagonal lattice with the in-plane cell length of 1.5 ± 0.1 nm. Plane indices shown in Figure 2.4c is fully consistent with the modelled kagome lattice structure and similar to **NiDT** nanosheets[1].

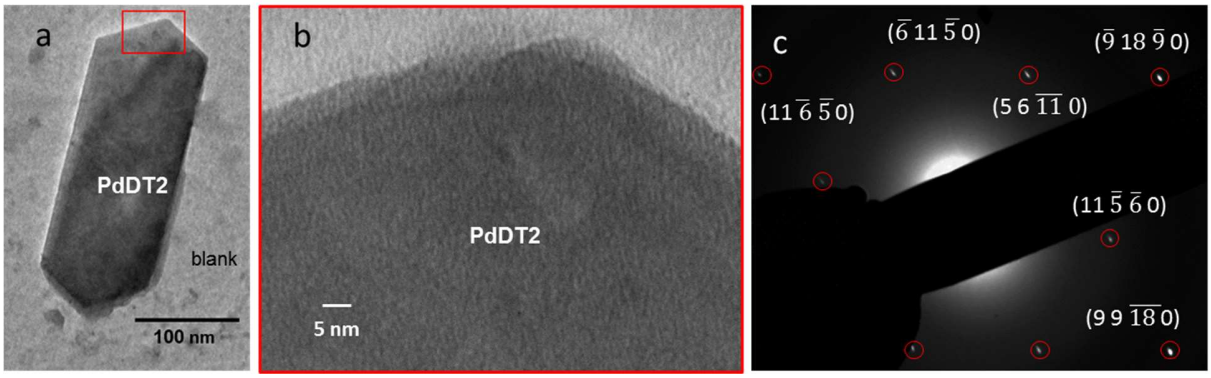

Figure 2.4 (a) TEM image of **PdDT2**, (b) magnified view of (a), and (c) its selected area electron diffraction (SAED) pattern.

2.5 Infrared (IR) Spectroscopy of PdDT2

In the IR spectrum of **PdDT2** (Figure 2.5), the strong S-H stretching vibration of BHT disappears completely. In addition, the broad C–S• stretching peak is observed at 1029 cm^{-1}. Mononuclear complex $Pd(L^{Bu})_2$ features three C–S• stretching peaks in the region of 1000-1100 cm^{-1} at the 0 oxidation state, whereas they change to a single peak at 1102 cm^{-1} in the –1 oxidation state[1,5–7]. The observed broad peak at 1029 cm^{-1} assures that the 0 oxidation state is major in **PdDT2**.

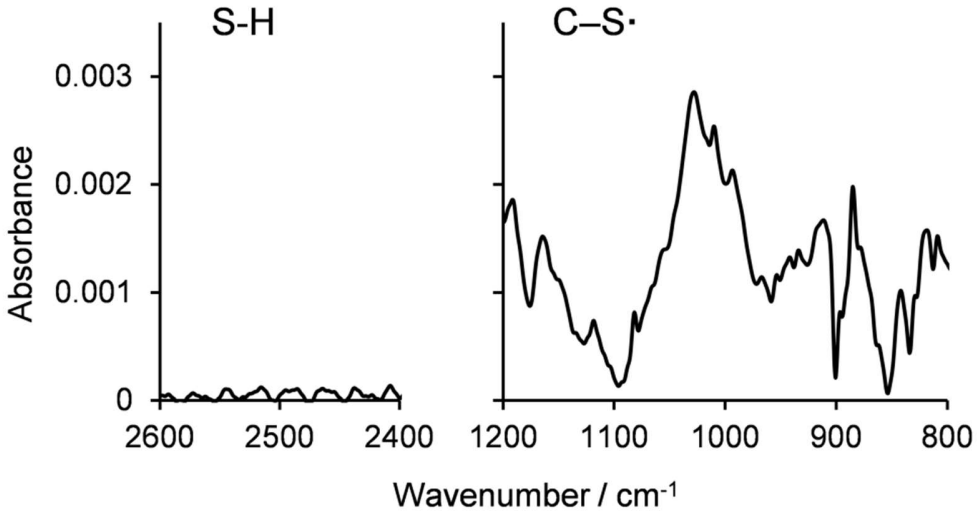

Figure 2.5 IR spectra of BHT compared with **PdDT2**.

2.6 X-ray Photoelectron Spectroscopy of PdDT2

XPS analysis of **PdDT2** reveals the existence of each element (S, Pd, K) in Figure 2.6.1 and oxidation state of bis(dithiolato)palladium $[PdS_4]^n$ (n=0, -1) units is reflected in the binding energy of the S atom and is found by deconvolution of the S 2s envelope. Three deconvoluted bands emerge at 226.2, 227.7, and 232.6 eV for **PdDT2** Figure 2.6.2 and Table 2.1 The first two are due to the -1 and 0 oxidation states of the $[PdS_4]$ motif, respectively, while the broad band at 230.5 and 232.6 eV are assignable to a ‘‘shake-up’’ peaks[12,13], which are often observed in metal bis(dithiolene) complexes[1,8].

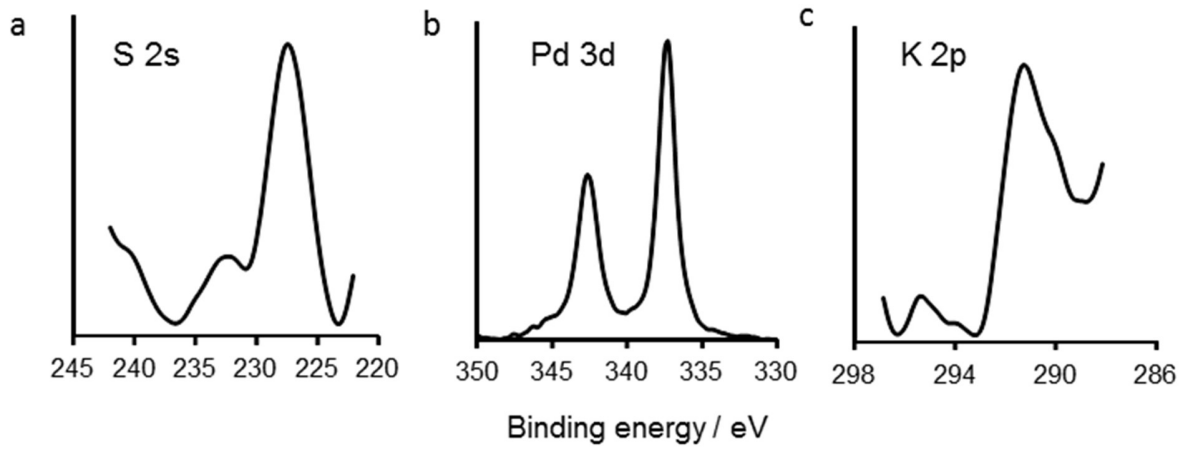

Figure 2.6.1 The S 2s (a), Pd 3d (b), K 2P (c) spectra of **PdDT2**.

Potassium ion is included as counter cation for both the anionic forms of **PdDT**, [bis(dithiolato)palladium(III)]$^-$. Deconvolution of the S 2s peak indicates that the [bis(dithiolato)palladium] unit is in the mixed valence state with 0 : –1 = 81 : 19 in **PdDT2**. We note that the valence is highly delocalized in **PdDT**, such that the oxidation number of the palladium bis(dithiolene) unit is uniform, adopting a value of –0.19. High ratio of the 0 oxidation state compared to **micro-NiDT**[1] (0 : –1 = 74 : 26) is probably from the effect of the oxidant added in the aqueous layer. Additionally, metal bis(dithiolene) complexes have their redox properties predominantly on the ligand center[5]. From these features, **PdDT2** is suggested to possess the

mixed valence state of 0 and –1 similar to nickelladithiolene nanosheets (**micro-NiDt** and **nano-NiDt**)[2-1].

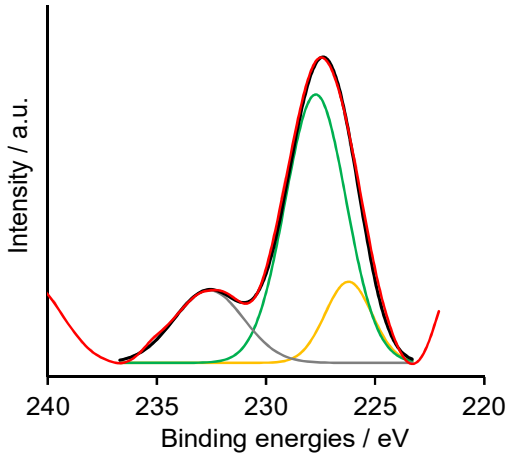

Figure 2.6.2 Deconvolutions of the S 2s peaks of **PdDT2**. The yellow and green Gauss curves are derived from the palladium bisdithiolene moieties with -1 and 0 oxidation states [1,3-6], respectively. The gray one is assigned to the "shake-up" peak, which is often observed in bisdithiolene complexes[12,13].

Table 2.1 Details of Deconvoluted S 2s XP Spectra

	Band	**Position (eV)**	**FWHM (eV)**	**Area (%)**
S2s band of **PdDT2**	1	226.2	2.5	15.0
	2	227.7	3.3	64.9
	3	232.6	3.7	20.1

2.7 Cyclic Voltammogram of **PdDT1** and **PdDT2**

In fact, redox potentials in 0/–1 oxidation states of mononuclear complexes $M^{II}(LBu)_2$ (M = Ni, Pd; LBu = 3,5-di-tert-butylbenzene-1,2-dithiolate ligands) are almost the same (–0.23 and –0.22 V vs ferrocenium/ferrocene)[5]. These data demonstrate that redox occurs on the ligand, and is nearly independent of the central metal ion Ni or Pd. The cyclic voltammograms of **PdDT1** and **PdDT2** on HOPG are shown in Figure 2.7. A reversible redox wave was observed at 0.18 V and 0.27 V vs Ag^+/Ag, which is ascribed to the 0/−1 redox couple of [PdS_4] unit[1,6]. The wave derived from the -1/-2 couple was not observed in the available potential window which is common for monomeric dithiolene complex[5]. At high scan rate, both reduction and oxidation waves disappear implying that the electron transfer is very sluggish between reduced and oxidized palladium bis(dithiolene) motif of oxidation state -1 and 0, respectively.

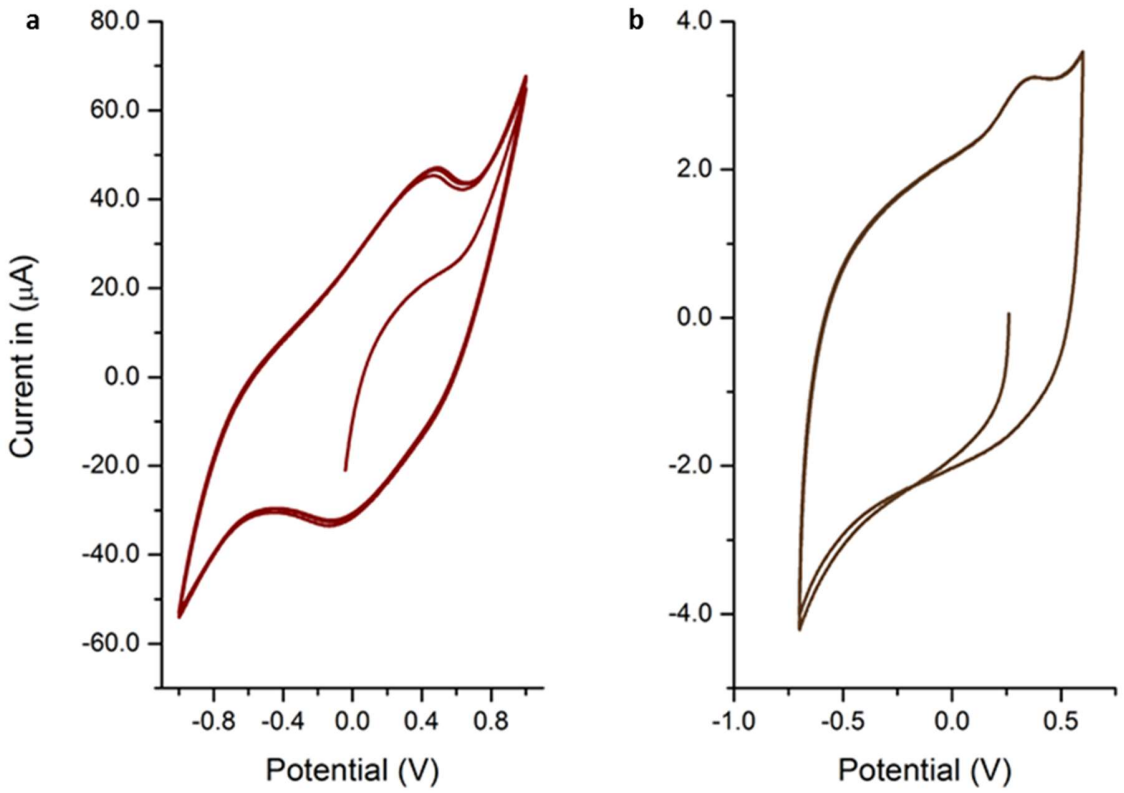

Figure 2.7 Cyclic voltammograms[1,6] **PdDT1** (a) and **PdDT2** (b) on ITO and HOPG, respectively, in 0.1 M Bu_4NPF_6 in dichloromethane.

2.8 Single Layer of Palladium Bis(dithiolene) CONASH

2.8.1 Synthesis by Gas-Liquid Interfacial Reaction of nano-PdDT

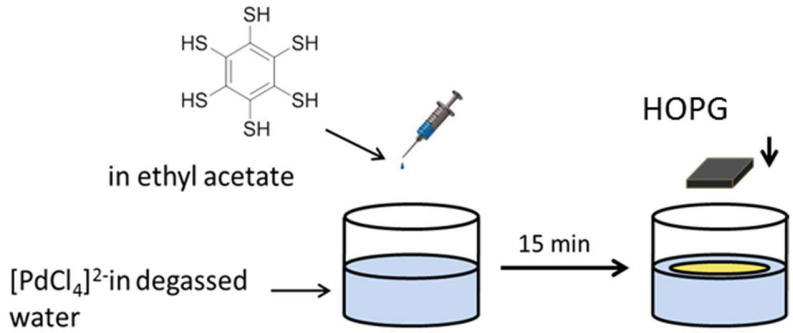

Figure 2.8.1 Synthesis of **nano-PdDT**.

The pristine surface being interesting site for reactions, thinner films can be anticipated via gas-liquid interfacial reactions. For nanoscience, control in the thickness is very important criteria. As explained previously, that the liquid-liquid interfacial reaction do not give control over the thickness in nm scale film formation. While spreading measured amount of ligand dissolved in ethyl acetate on surface of aqueous solution containing metal ion, the thickness of nanosheet in nm level can be controlled by the concentration of the ligand and the time of reaction.

BHT (30.4 μM) was gently spread to the surface (20.3 cm^2) of an aqueous solution of K_2PdCl_4 (1 mM). The amount of BHT was restricted, so that it covered 30% - 70% of the aqueous surface area. The area covered with BHT was calculated using the space-filling model. After 15 minutes of standing time, **nano-PdDT** was deposited on a clean HOPG substrate by bringing the substrate close to the interface in the vertical direction (Langmuir-Schaefer (LS) method). The HOPG was then gently immersed in water, followed by ethanol and then ethyl acetate. It was then dried in vacuo for 48 hours. The samples for STM measurements were prepared by the same method as **nano-PdDT** but BHT covered 30% of the aqueous surface.

2.8.2 Atomic Force Microscopy (AFM) of nano-PdDT

A 2-D sheet like morphology can be seen under AFM. The structure can be clearly distinguished from the bare HOPG substrate in the AFM topographic image. However, small white spots ascribed to PdNPs are observed under AFM. I failed to find monolayers in the AFM image, instead, few layered nanosheet of 4 nm-10 nm were seen. This is probably due to severe π-π stacking between nanosheets.

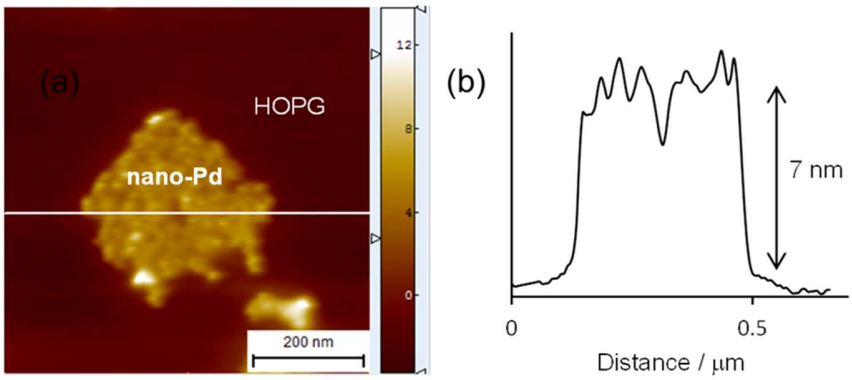

Figure 2.8.2 AFM image of **nano-PdDt**. (a) AFM height image of topography image. (b) its cross-sectional analysis in (a).

2.8.3 Scanning Tunnelling Microscopy (STM) of nano-PdDT

Scanning probe microscopy (SPM) was exploited to determine the structure of atomically thin layered nanosheets. Thin sheets of **nano-PdDT** can be detected by STM as well as AFM measurements (Figure 2.8.2). Yet, by STM analysis I observed hexagonal patterns. The periodicity in STM image (Figure 2.8.3.1) of the hexagonal patterns (7.75 nm) was too large to be assigned directly to the in-plane lattice of **nano-PdDT** (1.5 ± 0.1 nm from (SAED) for **PdDT2**) nor for HOPG (0.246nm)[1]. Hence, the hexagonal periodicity observed is a moiré pattern conformed by superimposition of two lattices: one is the in-plane of **nano-PdDT** and the other is derived from HOPG resulting the formation of a super lattice with a relative orientation angle of 1.78° (Figure 2.8.3.2). The same resulting periodicity can be simulated, which confirms that the moiré pattern is indeed due to the overlap between HOPG and **PdDT** CONASH.

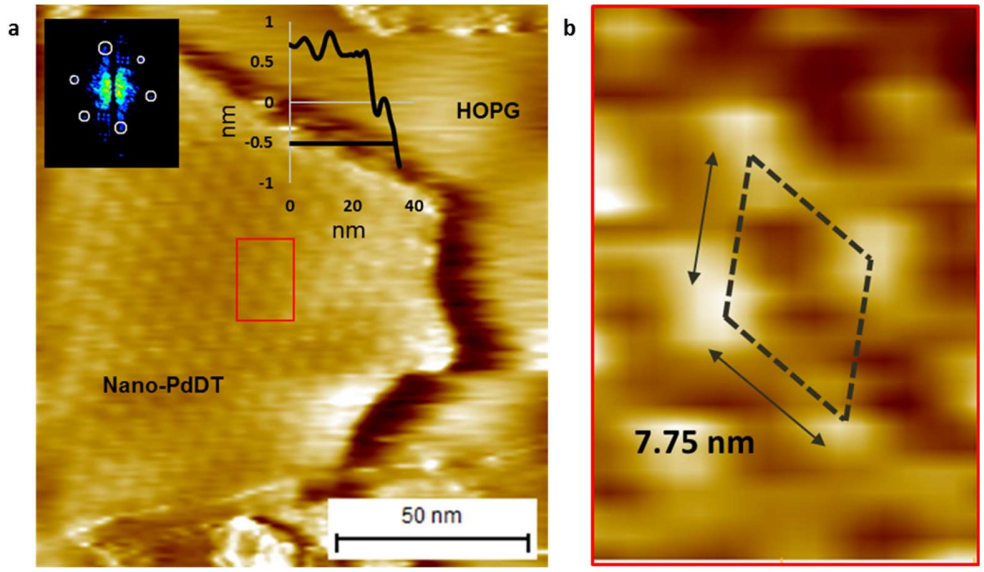

Figure 2.8.3.1 (a) STM image of single layer nanosheet; Tip bias (V_{tip}) = -300 mV, (inset) Fast Fourier Transform (FFT) of STM image, (b) magnified of area marked in (a).

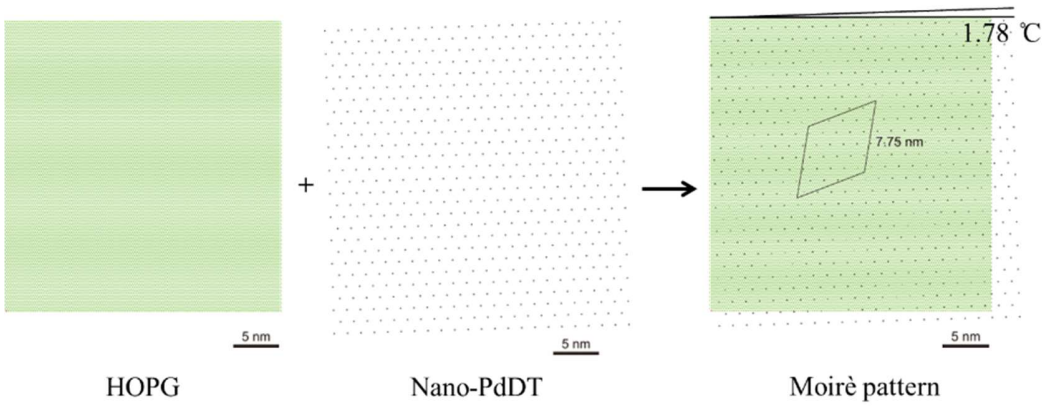

Figure 2.8.3.2 Formation of moiré pattern from two hexagonal periodicity

2.9 Experimental Section

Materials

K_2PdCl_4 was purchased from Kanto Chemical Co., Inc. NaBr was received from Wako Pure Chemical Industries, Ltd. Dichloromethane and ethyl acetate were distilled from NaH under a nitrogen atmosphere, and were stored with molecular sieves (4A, 1/16). Water was purified using the Milli-Q purification system (Merck KGaA). Benzenehexathiol (BHT)[10] was synthesized according to the literature.

Substrate preparations

HOPG was purchased from Alliance Biosystems, Inc. (Grade SPI-1 10 × 10 × 2 mm) and cleaved with adhesive tape just before use. Silicon wafers (P-doped with a concentration of $3 \times 10^{18} cm^{-3}$) with thermally grown 100 nm-thick SiO_2 were purchased from Yamanaka Semiconductor, and cut into squares (1 × 1 cm). HMDS treatment was carried out in a petri dish. A silicon wafer was immersed in an ethanol solution (10 mL) of HMDS (100 μL) for 1 day. After annealing at 130℃ for 2 min, the wafer was rinsed with ethanol and dried *in vacuo*.

Synthesis of PdDT1

Under an argon atmosphere, to 1.2–1.5 mg of BHT, degassed dichloromethane (10 mL) was added in a N_2 purged glass vial with a diameter of 30 mm, to prepare a saturated solution (~0.24 mM) followed layering with degassed pure water (10 mL) to form a double layer. A degassed aqueous solution (10 mL) containing K_2PdCl_4 (5 mM) and NaBr (1 mM) was added to the water phase. After waiting for 1 day, **PdDT1** emerged at the interface as a black solid with a metallic luster. After the removal of the aqueous and organic phases, sample was washed thoroughly with water, ethanol, and dichloromethane, and dried in *vacuo* at 150°C to give lustrous black powder.

Synthesis of PdDT2

Under an argon atmosphere, to 1.2–1.5 mg of BHT, degassed dichloromethane (10 mL) was added in a N_2 purged glass vial with a diameter of 30 mm, to prepare a saturated solution (~0.24 mM) followed layering with degassed pure water (10 mL) to form a double layer. A degassed aqueous solution (10 mL) containing $K_3[Fe(CN)_6]$ (1mM) and K_2PdCl_4 (5 mM) were added to the water phase. After waiting for 1 day, **PdDT2** emerged at the interface as a black solid with a metallic luster. After the removal of the aqueous and organic phases, the sample was washed thoroughly with water, ethanol, and dichloromethane, and dried in *vacuo* at 150°C to give lustrous black powder.

Characterisation

The TEM samples were prepared by depositing **1** and **2** on a copper grid, using ethanol suspension. IR-ATR spectra were recorded using Jasco FT/IR-6100 at room temperature under vacuum. XPS data were obtained using PHI 5000 VersaProbe (ULVAC-PHI, INC.). Al Kα (15 kV, 25 W) was used as the X-ray source, and the beam was focused on a 100-μm^2 area. The spectra were analysed using MultiPak Software, and data calibrated using the C1s peak at 284.6 eV. SPM measurement was carried out using Agilent Technologies 5500 Scanning Probe Microscope, under an ambient condition. AFM was performed in the high-amplitude mode (trapping mode), with silicon cantilever PPP-NCL (Nano World). Probes for STM were cut from a wire (Pt-Ir alloy, 4:1, 0.25 mmϕ) and chemically etched in 0.1 M NaOH solution with Pt as the counter electrode, to obtain a sharp tip. Electrochemical measurements were recorded using ALS 650DT electrochemical analyzer (BAS. Co., Ltd.). A homemade Ag^+/Ag reference electrode (0.01 M $AgClO_4$ in 0.1 M Bu_4NClO_4/acetonitrile) and a Pt wire counter electrode were implemented in order to establish a three-electrode system. Bu_4NPF_6, acting as a supporting electrolyte, was recrystallized from EtOH and put under vacuum for 24 hours.

2.10 References

1. Kambe, T., Sakamoto, R., Hoshiko, K., Takada, K., Miyachi, M., Ryu, J. H., Sasaki, S., Kim, J., Nakazato, K., Takata, M. & Nishihara, H. π-Conjugated nickel bis(dithiolene) complex nanosheet. *J. Am. Chem. Soc.* **135**, 2462–2465 (2013).

2. Kambe, T., Sakamoto, R., Kusamoto, T., Pal, T., Fukui, N., Hoshiko, K., Shimojima, T., Wang, Z., Hirahara, T., Ishizaka, K., Hasegawa, S., Liu, F. & Nishihara, H. Redox control and high conductivity of nickel bis(dithiolene) complex π-nanosheet: A potential organic two-dimensional topological insulator. *J. Am. Chem. Soc.* **136**, 14357–14360 (2014).

3. Cui, J. & Xu, Z. An electroactive porous network from covalent metal-dithiolene links. *Chem. Commun.* **50**, 3986–3988 (2014).

4. Hamoudi, H. Carbon – metal nanosheets from the water – hexane interface. *J. Mater. Chem. C* **3**, 3636–3644 (2015).

5. Ray, K., Weyhermuller, T., Neese, F. & Wieghardt, K. Electronic structure of square planar bis(benzene-1,2-dithiolato)metal complexes $[M(L)_2]^z$ (z = 2-, 1-, 0; M = Ni, Pd, Pt, Cu, Au): an experimental, density functional, and correlated ab initio study. *Inorg. Chem.* **44**, 5345–5360 (2005).

6. Matsuoka, R., Sakamoto, R., Kambe, T., Takada, K., Kusamoto, T. & Nishihara, H. Ordered alignment of a one-dimensional π-conjugated nickel bis(dithiolene) complex polymer produced via interfacial reactions. *Chem. Commun.* **50**, 8137–8139 (2014).

7. Liu, B., Qiao, W. & Wang, Z. Y. Colorless metallodithiolene oligomers and polymers with intense near- and mid-infrared absorption. *RSC Adv.* **5**, 6815–6822 (2015).

8. Sellmann, D., Binder, H., Häußinger, D., Heinemann, F. W. & Sutter, J. Transition metal complexes with sulfur ligands Part CXLIV. Square planar nickel complexes with NiS_4 cores in three different oxidation states: Synthesis, X-ray structural and spectroscopic studies. *Inorganica Chim. Acta* **300-302**, 829–836 (2000).

9. Haynes, W. M., Lide, D. R., Bruno, T. J. CRC Handbook of Chemistry and Physics, CRC Press, **95th Edition**, 12-17 (2014).

10. Harnisch, J. A. & Angelici, R. J. Gold and platinum benzenehexathiolate complexes as large templates for the synthesis of 12-coordinate polyphosphine macrocycles. *Inorganica Chim. Acta* **300-302**, 273–279 (2000).

11. Faust, T. B., Usov, P. M., D'Alessandro, D. M. & Kepert, C. J. Highly unusual interpenetration isomers of electroactive nickel bis(dithiolene) coordination frameworks. *Chem. Commun.* **50**, 12772–4 (2014).

12. Liu, S.-G., Liu, Y.-Q. & Zhu, D.-B. Preparation and spectral properties of new molecular conductors based on anion salt. *Synth. Met.* **89**, 187–191 (1997).

13. Zhou, S., Ichimura, K. & Inokuchi, H. X-Ray photoelectron spectroscopy characteristics of a novel organic semiconductor BTQBT and its derivatives. *J. Mater. Chem.* **5**, 1725 (1995).

Chapter 6

Concluding Remarks and Future Prospective

The thesis begins with quantum confinement and its importance regarding the availability of the discrete energy levels that of the bulk energy bands. Having said that, 2-D materials have gained much attention because of it is tunable energy distribution by several routine methods for the required achievable practical applications. I have classified the 2-D layered materials according to its composition and discussed briefly about their present attainable research. But depending on the above classified forms of 2-D layered materials, there is a lack of use of entire periodic table as a result, most of the top-down and bottom-up approaches have their own limitations at the point of element selection, corresponding reactivity and stability of such materials. The other considerable easy approach is discussed in the first Chapter as exploitation of coordination Chemistry. Few of such interesting reports are briefly discussed along with the importance of surface reactions. Later at the end of the Chapter, I briefly formulate the pros and the cons of using the benzene hexathiol (BHT) ligand as a coordinating ligand with late transition metals of Group 10 as my research plan.

In Chapter 2, interfacial reaction between the Pd-metal solution and ligand was conducted resulting into formation of coordination nanosheet with simultaneous formation of metallic palladium. The pure sheets are obtained by addition of oxidizing agent, hexacyanoiron (III) salts, which act as a redox buffer inhibiting the formation of metallic palladium from its corresponding Pd^{2+} salt precursor. In this case the reduction potential of BHT is not altered. Stacked and few layer sheet are characterized with the help of different microscopy, X-ray photoelectron (XP) and IR spectroscopies technique. The nanosheet is mixed valent of 0 and -1 and is confirmed by XP spectroscopy and cyclic voltammetry. Hence, Chapter 2 shows the successful formation of the 2-D layered palladium bis(dithiolene) coordination nanosheets.

Hence, these studies pave a synthetic procedure to be used for thiol based ligands with late transition metals having high positive reduction potential, thereby integrating interesting ligand design to explore new physical properties in near future.

Acknowledgement

The thesis owes its present form to several ones who have significantly supported mentally and physically; without whom this would not be possible. I express my gratitude to all of them.

Firstly, I am deeply indebted to Professor Dr. Hiroshi Nishihara who has been a constant source of encouragement and enthusiasm in the research projects I have taken on. I appreciate all his time, ideas and contributions to make my research productive. I am honored to be a part of his group.

I am very much thankful to Assistant Professor Dr. Tetsuro Kusamoto for the humble discussions and the excellent advice on technical difficulties I have faced, mostly regarding my experiments. I sincerely thank Assistant Professor Dr. Ryota Sakamoto for his kind directions and innovative ideas.

I am grateful to Project Assistant Professor Dr. Hiroaki Maeda and Project Assistant Professor Dr. Mariko Miyachi for their extended technical help and support when I faced troubles.

I take this opportunity to thank Associate Professor Dr. Yoshinori Yamanoi and Project Assistant Professor Dr. Kuo Hui Wu for their encouragement. I personally thank Dr. Maw Lin Foo for his constant words of encouragement even at the tough times of my Ph. D. pursuit.

I sincerely thank Professor Dr. Kazuo Nakazato and Dr. Nissar Mohammad Karim in Nagoya University for designing the digited gold electrode for conductivity measurements.

Many researchers technically extended their support. I appreciate Dr. Kohei Okitsu in Research Hub for Advanced Nano Characterizations in School of Engineering (The University of Tokyo) for XPS measurement; Ms. Kimiyo Saeki and Ms. Aiko Kamitsubo in School of Science (The University of Tokyo) for elemental analysis; Dr. Naoya Fukui for measuring the conductivity.

I am also thankful to the lab members, especially the CONASH research group: Dr. Tetsya Kambe, Mr. Ken Hoshiko, Mr. Xinsen Sun, Ms. Eunice Jia Han Phua, Mr. Toshiki Yagi, Mr. Choon Meng Tan, Mr. Toshiki Iwashima, Mr. Cao Jian, Mr. Ukyo Nakajima and Ms. Ma. Leah Maramara for their help and constant discussions. I should take this opportunity to thank Dr. Kenji Takada, Mr. Ryota Matsuoka in particular for teaching me several techniques in this laboratory; it was a pleasure to learn from them. Besides, I am thankful to other lab members for their positive vibes and heart felt support including Dr. Yohei Hattori, Dr. Takamasa Tsukamoto, Ms. Mustafar

Suzaliza, Mr. Mizuho Tsuchiya, Mr. Masaki Shimada, Ms. Yasuya Ogino, Ms. Risa Aoki, Ms. Aayushi Bajpayee, Ms. Chie Ohde, Mr. Shinya Koga, Mr. Ryojun Toyoda, Mr. Amane Ohkubo, Mr. Shun Kimura, Mr. Daiki Nishiori, Mr. Tadashi Iokawa, Mr. Tsukasa Usuki, Mr. Ryo Shiotsuki, Mr. Uki Tani and Mr. Takuwa Tsuji.

My time at Todai was largely spent with my friends in particular Keisuke Wada, Amalia Rapakousiuo and Julius F. Koegel who have been with me in tough times with their positive approaches that made me strong in every instance.

I am indebted to the Todai-IIT Scholarship and the staffs who put endless effort to process my documents. Most figures in Chapter 2 were reproduced from my publication in ChemPlusChem in 2015. I thank Wiley Publishers for allowing me to reuse them in this thesis.

At the last, my deepest gratitude to my family for their unflagging love and unconditional support throughout my studies especially to my father, Dr. Gunendra Prasad Pal and my mother, Mrs. Anju Pal to let me live the unique carefree childhood. My sincere gratitude to my dearest uncle, Dr. Dipti Prakas Pal, for everything that I am and I perceive today.

I appreciate you all.

Tigmansu Pal

The University of Tokyo

July 2016

【Publication(s) related to the thesis】

1. "Interfacial Synthesis of Electrically Conducting Palladium Bis(dithiolene) Complex Nanosheet," Tigmansu Pal, Tetsuya Kambe, Tetsuro Kusamoto, Maw Lin Foo, Ryota Matsuoka, Ryota Sakamoto, Hiroshi Nishihara *ChemPlusChem* 2015, *80*, 1255-1258.

【Publication(s) not related to the thesis】

1. "The coordination nanosheet (CONASH)," Ryota Sakamoto, Kenji Takada, Xinsen Sun, Tigmansu Pal, Takamasa Tsukamoto, Eunice Jia Han Phua, Amalia Rapakousiou, Ken Hoshiko, Hiroshi Nishihara "The coordination nanosheet (CONASH)" *Coord. Chem. Rev.* 2016, in press.
2. "Syntheses and solid state structures of various Zinc (II) Complexes withBi-dentate *N*-(Aryl)imino-Acenapthenone (Ar-BIAO) Ligands," Srinivas Anga, S. Rej, K. Naktode, T. Pal and Tarun K. Panda *J. Chem. Sci*., 2015, *127*, 103-113.
3. "Redox Control and High Conductivity of Nickel Bis(dithiolene) Complex &pi-Nanosheet: A Potential Organic Two-Dimensional Topological Insulator," Tetsuya Kambe, Ryota Sakamoto, Tetsuro Kusamoto, Tigmansu Pal, Naoya Fukui, Takahiro Shimojima, Zhengfei Wang, Toru Hirahara, Kyoko Ishizaka, Shuji Hasegawa, Feng Liu, Hiroshi Nishihara *J. Am. Chem. Soc.* 2014, *136*, 14357-14360.
4. "Synthesis, Crystal Structure and Reactivity Study of NPyrrolyl-P,P-Diphenylphosphino Sulfide/Selenide Ligand," Srinivas Anga, Tigmansu Pal, Tarun K. Panda *Journal of Modern Chemistry & Chemical Technology*, 2014, *5*, 35-45.
5. "Cationic Copper (I) Complexes with Bulky 1,4-Diaza-1,3-Butadiene Ligands - Synthesis, Solid State Structure and Catalysis," Srinivas Anga, Ravi K. Kottalanka, Tigmansu Pal and Tarun K. Panda *Journal of Molecular Structure*, 2013, *1040*, 129-138.
6. "Synthesis and Structures of Dimeric Zinc Complexes Supported by Unsymmetrical Rigid Bidentate Imino-acenapthenone Ligand," Srinivas Anga, Tigmansu Pal, Ravi K. Kottalanka, Mitali Paul, and Tarun K. Panda *Canadian Chemical Transactions*, 2013, *1*, 105-111.